Geomorphology of the Makgadikgadi Basin (Botswana): Insight Into the Propagation of the East African Rift System

Louis Gaudaré, Olivier Dauteuil, Marc Jolivet

Tectonics®

RESEARCH ARTICLE
10.1029/2023TC007988

Geomorphology of the Makgadikgadi Basin (Botswana): Insight Into the Propagation of the East African Rift System

Louis Gaudaré[1], Olivier Dauteuil[1], and Marc Jolivet[1]

[1]Géosciences-Rennes, UMR-CNRS 6118, University of Rennes, Rennes, France

Key Points:

- Geomorphic indicators better constrain kinematics and deformation relative chronology of the Makgadikgadi Rift Zone (MRZ), Botswana
- Low activity of the MRZ suggests that present-day rift activity shifts from the Mid-Zambezi Rift to the Okavango Graben
- We propose a NE-SW propagation model of the East African Rift System at its southwestern terminus driven by plates relative motions

Supporting Information:

Supporting Information may be found in the online version of this article.

Correspondence to:

L. Gaudaré,
louis.gaudare@univ-rennes.fr

Citation:

Gaudaré, L., Dauteuil, O., & Jolivet, M. (2024). Geomorphology of the Makgadikgadi Basin (Botswana): Insight into the propagation of the East African Rift System. *Tectonics*, *43*, e2023TC007988. https://doi.org/10.1029/2023TC007988

Received 28 JUN 2023
Accepted 8 JAN 2024

Author Contributions:

Conceptualization: Louis Gaudaré, Olivier Dauteuil, Marc Jolivet
Data curation: Louis Gaudaré
Formal analysis: Louis Gaudaré, Olivier Dauteuil, Marc Jolivet
Investigation: Louis Gaudaré, Olivier Dauteuil, Marc Jolivet
Methodology: Louis Gaudaré, Olivier Dauteuil, Marc Jolivet
Supervision: Olivier Dauteuil, Marc Jolivet
Writing – original draft: Louis Gaudaré

Abstract The Southwestern Branch of the East African Rift System propagates through the Central and Southern African plateaus and ends in the Okavango Makgadikgadi Zambezi Basin. This basin hosts the Okavango Graben and the Eiseb Graben, considered as the terminus of the Southwestern Branch of the rift. To the southeast, the Makgadikgadi Basin is affected by a series of normal faults forming the Makgadikgadi Rift Zone (MRZ) which regional geodynamic significance remains unclear. Based on fieldwork and geomorphic analysis, we revisited the geomorphological features associated with paleolakes and the fault pattern within the Makgadikgadi Basin to better constrain the dynamics of the MRZ. Fault scarps and offsets along linear dunes show normal-dip kinematics of faults, indicating a NW-SE extension direction in the area. Furthermore, lacustrine shorelines in the basin are undeformed, proving that they post-date the fault activity. The previously published ages of these shorelines demonstrate that the MRZ currently has a low tectonic activity. Integrated in the geodynamic framework of the region, these results suggest that present-day deformation shifts toward the Okavango Graben north of the MRZ. We therefore propose a "zip-opening" model to explain the propagation of the Southwestern Branch of the East African Rift System where the tip of the system progressively progresses southwestward, driven by motions of the continental plates.

1. Introduction

The East African Rift System (EARS) is an active zone of continental extension splitting the eastern part of the African continent (e.g., Chorowicz, 2005; Macgregor, 2015; Saria et al., 2014). Its opening initiated in the Afar during the Paleogene and propagated southward through several branches, defining embryonic boundaries of continental plates (Daly et al., 2020; Martin, 2023; Saria et al., 2014; Simon, 2015; Stamps et al., 2008, 2021) (Figure 1a). In Southern Africa, the Okavango Graben and its southwestern prolongation, the Eiseb Graben, are considered as forming the present-day terminus of the southwestern extension of the EARS (e.g., Modisi, 2000; Wanke, 2005), which propagates along the southern margin of the Central African Plateau and through the Kalahari Plateau (Daly et al., 2020) (Figure 1b). This area thus represents a case example to better constrain the deformation processes at play during the early stages of rift opening (Kinabo et al., 2007). The mechanisms and chronology of the rift propagation in this region are poorly constrained. Geodetic data suggest a plate boundary passing through and beyond the Okavango and Eiseb grabens (Malservisi et al., 2013; Wedmore et al., 2021). However, there is no clear evidence of surface deformation supporting that the EARS track extends westward toward the Namibian margin (Hasterok et al., 2022). Moreover, several studies showed that the deformation is not restricted to the Okavango and Eiseb grabens but also affects the adjacent Makgadikgadi Basin to the southeast (Moore et al., 2012; Pastier et al., 2017; Reeves, 1972a; Scholz et al., 1976) where a series of normal faults forms the Makgadikgadi Rift Zone (MRZ) (Baillieul, 1979; Eckardt et al., 2016) (Figure 1b). The relationships between deformation in the Okavango Graben and the MRZ have been little investigated, nor the links between these two features and the EARS-related Mid-Zambezi Rift to the northeast. Better understanding these relationships would provide new insights into the EARS propagation in particular and the evolution of rifts in general.

The Okavango Graben, the Eiseb Graben and the Makgadikgadi Basin belong to a wide low-elevation area of the Kalahari Plateau called the Makgadikgadi-Okavango-Zambezi Basin (MOZB) (Haddon & McCarthy, 2005; Ringrose et al., 2005) (Figures 1b and 2a). The MOZB as a whole is often considered an EARS-related depression (e.g., Franchi et al., 2022; Riedel et al., 2014; Ringrose et al., 2005; Schmidt et al., 2017). However, most of the studies only focus on the Okavango Graben whereas links between the EARS and the Makgadikgadi Basin remain understudied. Furthermore, faults of the MRZ affect the Makgadikgadi Basin but it has never been demonstrated that they were at the origin of the Makgadikgadi topographic depression. Other processes, unlinked to EARS propagation, have also been proposed to explain the formation of this depression, such as epeirogenic

Writing – review & editing: Olivier Dauteuil, Marc Jolivet

uplift along a flexural axis (Haddon & McCarthy, 2005; Moore & Larkin, 2001; Moore et al., 2012). Thus, a better understanding of the tectonic movements within the Makgadikgadi Basin is necessary to better constrain its links with the EARS.

The almost ubiquitous Quaternary sedimentary cover in the MOZB makes for poor outcrop conditions, hindering tectonic studies with classical field markers such as fault planes and striations (e.g., Modisi, 2000). Thus, tools other than direct field observations have to be used to determine fault's kinematics and chronology. In this work, we focus on the structural pattern and geomorphology of the Makgadikgadi Basin to propose an innovative propagation model of the EARS at its southwestern terminus. We (a) conduct a remote sensing study to map the faults and lineaments at the Makgadikgadi Basin scale, (b) describe the morphological characteristics of faults and lineaments based on field observations and elevation data and (c) bring new constraints on fault kinematics and chronology based on their geometric relationships with geomorphic features in the basin.

2. Geological and Geomorphological Settings

2.1. The Southwestern Terminus of the East African Rift System

In its northern part, the EARS is composed of a single corridor, the Main Ethiopian Rift, going from Afar to the Lake Turkana region. There, it splits into two branches: the Eastern Branch crossing Kenya and Tanzania and the Western Branch going from Lake Albert to Lake Tanganyika (e.g., Chorowicz, 2005) (Figure 1a). The Southwestern Branch of the EARS corresponds to a network of separate basins prolonging the rift system down to the Okavango and Eiseb grabens (Figure 1b). Propagation of the Southwestern Branch is estimated to have started during Plio-Pleistocene times and is still active today (Daly et al., 2020; Wedmore et al., 2021). The location of most of the basins in the Southwestern Branch, and in the EARS in general, is controlled by inherited basement structures, preferentially following Pan-African mobile belts and Mesozoic rift basins, avoiding cratons (e.g., Daly et al., 1989; Fairhead & Stuart, 1982; Kinabo et al., 2008; McCarthy et al., 1993; Morley, 2010). Recent tectonic and geodetic studies show that the Southwestern Branch of the EARS marks the separation between at least two distinct continental plates (Figure 1a): the Nubian plate to the northwest and the San plate to the southeast (Daly et al., 2020; Wedmore et al., 2021). A third distinct plate, the Angoni Plate, is also conjectured between the Lower Zambezi Rift, the Luangwa Rift and the Malawi Rift (Daly et al., 2020; Williams et al., 2021). The Okavango and Eiseb grabens are the southwestern-most surface features that can be related to the Southwestern Branch of the EARS. Consequently, no clear boundary separating the San and the Nubian plates can be delimited between the Eiseb Graben and the Namibian Margin (Hasterok et al., 2022). Daly et al. (2020) hypothesized three distinct scenarios: (a) that the Eiseb Graben is the tip of a boundary that has not yet propagated further west, (b) that the Nubian-San boundary links to the NNW fault systems in the Namibian Highlands or (c) that the Nubian-San boundary links to the Walvis Ridge in the Atlantic Ocean.

The MOZB is located at the southwestern tip of the Southwestern Branch of the EARS (Figure 1b). EARS-induced deformation in the MOZB had been first hypothesized by Du Toit (1927) and then inferred by Reeves (1972b) and Scholz et al. (1976) from a NE-SW seismicity axis affecting the region and parallel to linear morphologies in the Okavango Delta area and the Makgadikgadi Basin. The EARS-related features in the MOZB, namely the Okavango Graben, the Eiseb Graben and the MRZ, share a similar NE-SW trend but have different morphological and structural patterns. The Okavango Graben, to the northwest, is an active half-graben approximately 600 km long and 180 km wide, delimited by normal to dextral strike-slip faults (Bufford et al., 2012; Kinabo et al., 2008; McCarthy et al., 1993; Modisi, 2000; Pastier et al., 2017). Its main faults are the Thamalakane, the Chobe and the Kunyere southeast border faults and the Gumare northwest border fault (Figure 2a). To the southwest the Eiseb Graben comprises four sub-parallel main faults sharing similar orientations with the faults of the Okavango Graben, of which they are suspected to be the prolongation (Wanke, 2005). The Okavango and the Eiseb grabens are separated from the Makgadikgadi Basin by the NE-SW Ghanzi Ridge in the southeast. The Makgadikgadi Basin is located in a wide topographic depression (e.g., Moore et al., 2012), delimited to the north by a topographic ridge in the Hwange area, to the east by a topographic ridge delimiting the Limpopo watershed, to the south by the Kalahari Schwelle and to the west by the Ghanzi Ridge (Figures 1b, 2a, and 2b). Affecting the Makgadikgadi Basin, the MRZ corresponds to a deformation zone presenting faults forming a horst and graben topography (Baillieul, 1979; Eckardt et al., 2016). Based on topographic and aeromagnetic data, Eckardt et al. (2016) mapped faults in the northern part of the Makgadikgadi Basin and distinguished a NNE-SSW striking fault family from an ENE-WSW one. They also suggested that the deformation area is larger than their study zone, continuing southward into the Makgadikgadi Basin, and northward probably forming a continuum with the Mid-Zambezi Rift (Figure 2a).

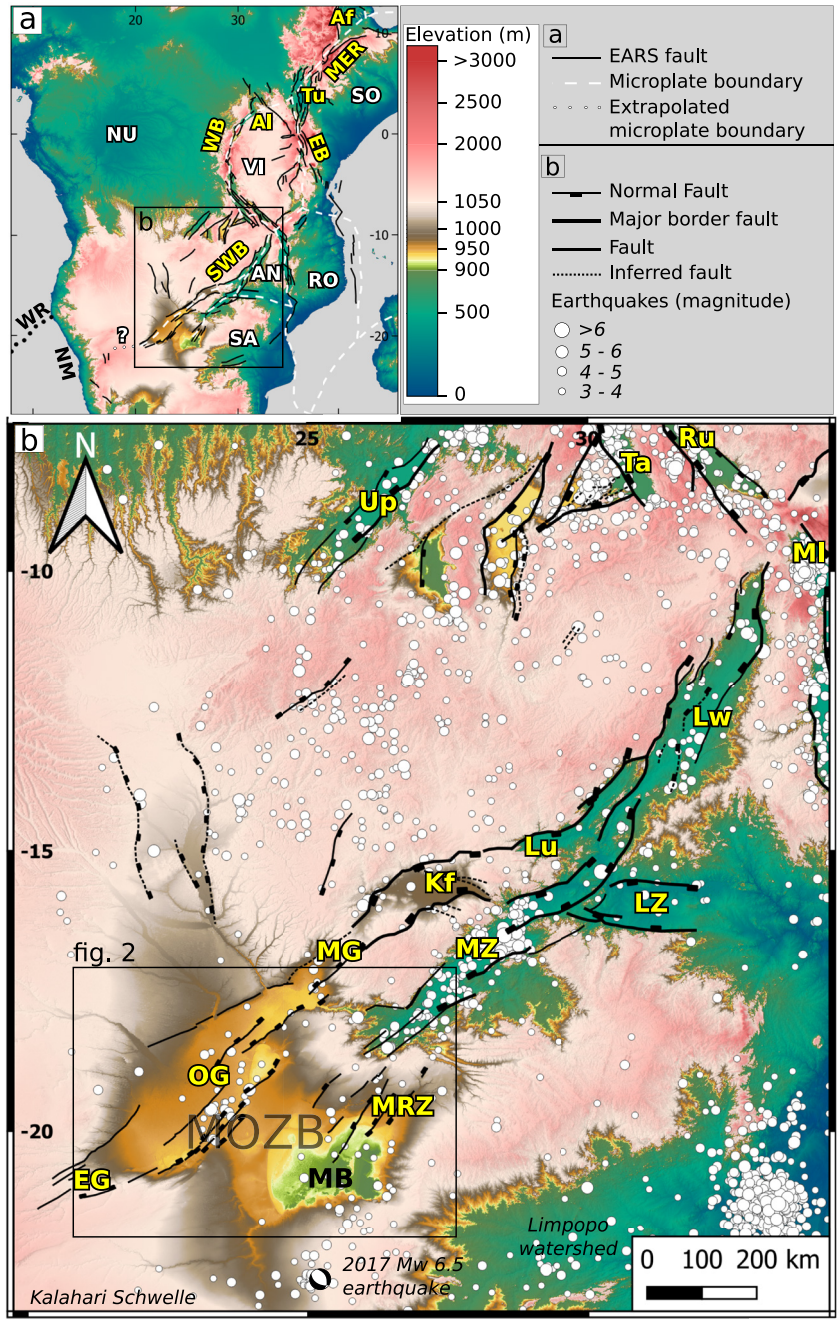

Figure 1. The East African Rift System (EARS). (a) Topographic map of the East African Rift System. White annotations correspond to embryonic plates from Daly et al. (2020): AN, Angoni microplate; NU, Nubian plate; RO, Rovuma microplate; SA, San plate; SO, Somalian plate; VI, Victoria microplate. The question mark points the current interrogation about the continuation of the boundary between San and Nubian plates toward the southwest. Yellow annotations correspond to locations along the EARS and black annotations correspond to other geological features mentioned in the text. Af, Afar; Al, Lake Albert; EB, Eastern Branch; MER, Main Ethiopian Rift; NM, Namibian Margin; SWB, South Western Branch; Tu, Lake Turkana; WB, Western Branch; WR, Walvis Ridge. (b) Topographic map and seismicity of the Southwestern Branch of the EARS. EG, Eiseb Graben; Kf, Kafue Graben; Lu, Luano Rift; Lw, Luangwa Rift; LZ, Low-Zambezi Rift; MB, Makgadikgadi Basin; MG, Machili Graben; Ml, Malawi Rift; MOZB, Makgadikgadi Okavango Zambezi Basin; MZ, Mid-Zambezi Rift; MRZ, Makgadikgadi Rift Zone; OG, Okavango Graben; Ru, Rukwa Rift; Ta, Tanganyika Rift; Up, Upemba Graben. Yellow annotations point rift segments. Seismic data come from International Seismological Centre (2022). The focal mechanism indicates the 2017 Mw 6.5 Moiyabana earthquake (Mulabisana et al., 2021). For (a) and (b) faults are compiled and modified from Chorowicz (2005), Daly et al. (2020), and Wanke (2005). Panels (a and b) share the same topographic symbology. Topographic data: Copernicus GLO-30 and GLO-90 DTED (ESA, 2019).

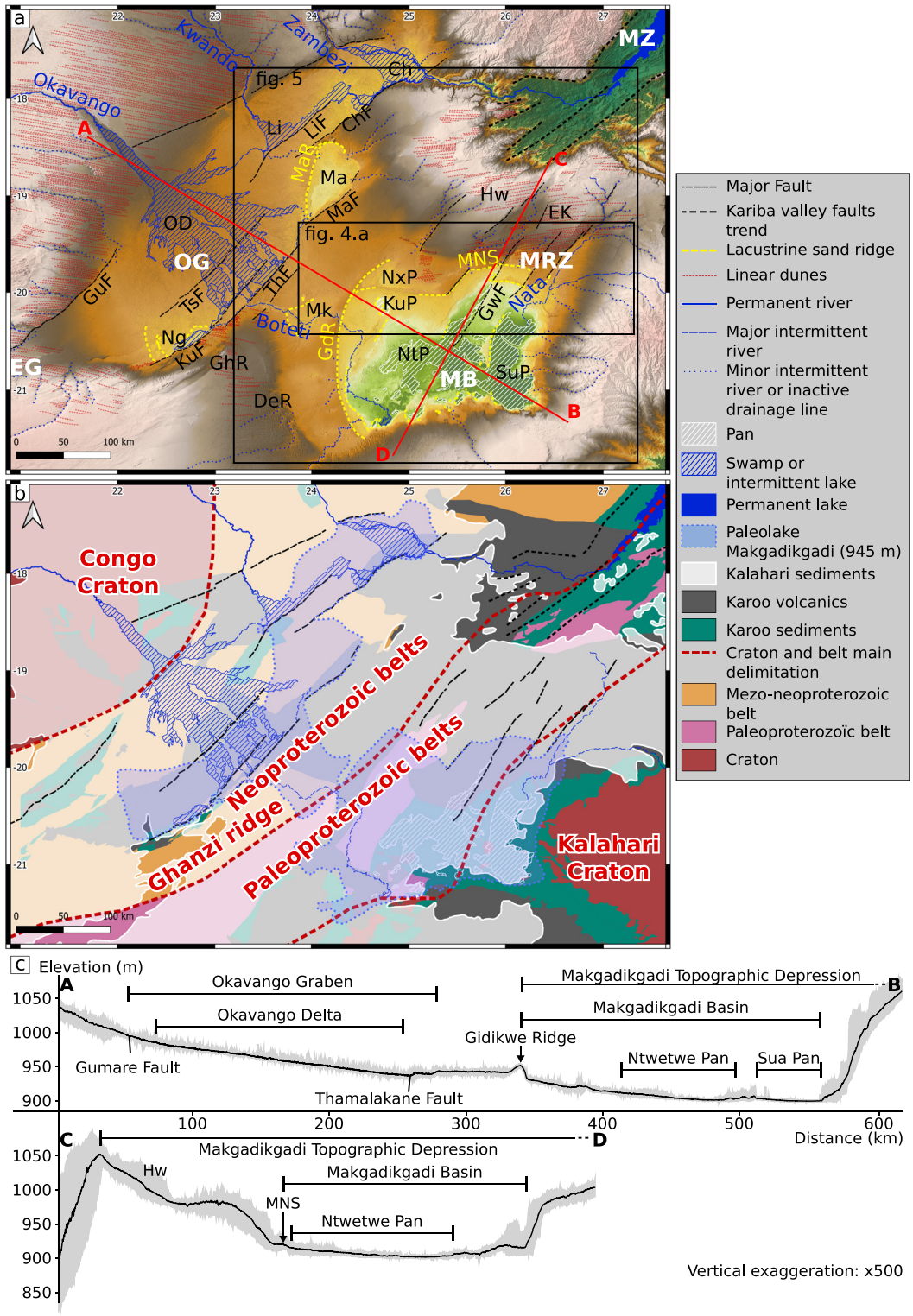

Figure 2.

The Mid-Zambezi Rift, extending from Mozambique to Eastern Botswana, is an active segment of the South-western Branch of the EARS (Figure 1b) with normal-slip active faults mainly striking NE-SW (Daly et al., 2020; Hlatywayo, 1995; Vail, 1968). A continuity between the Mid-Zambezi Rift and the MOZB tectonic structures has been suggested (e.g., Eckardt et al., 2016; McCarthy, 2013; Scholz et al., 1976), linking the MRZ and the

Okavango Graben to the EARS' segments located further north. However, the structural connection between the Okavango Graben, the MRZ and the Mid-Zambezi Rift remains poorly studied. On one hand, Daly et al. (2020) proposed that the Okavango Graben and the MRZ would belong to two separated corridors of the EARS (Figure 1b): the Okavango and Eiseb grabens would be the terminus of a corridor going through the Lake Rukwa Rift, the Luangwa Rift, the Luano Rift and the Kafue Graben, whereas the MRZ would be the end of a second corridor following the Mid-Zambezi Rift. On the other hand, Eckardt et al. (2016) suggested a tectonic continuity between the Mid-Zambezi Rift, the MRZ and the Okavango Graben based on their geographical proximity and mean fault-strike direction.

2.2. Seismicity of the Rift at Its Southwestern Terminus

The Mid-Zambezi Rift, the Okavango Graben and the Makgadikgadi Basin are seismically active but with significant differences in earthquakes frequencies and magnitudes (Figure 1b). No significant seismicity has been detected in the Eiseb Graben, despite Holocene tectonic activity being suspected (Wanke, 2005). The Mid-Zambezi Rift shows the strongest seismic activity in the region with an average frequency of ∼4 earthquakes per year reported since 1963 for magnitudes over 3 and a maximum magnitude of 6.5 measured in 1963 (International Seismological Centre, 2022). Part of the detected seismicity is induced by the Kariba artificial lake filling in the end of the 1950s. However, earthquakes reported prior to the construction of the dam and the fact that seismicity has not decreased significantly since the reservoir infill are evidence of high natural seismicity in the area (Dumisani, 2001). In the Okavango Graben, the seismic activity is mainly focused in the southeastern part, between the Thamalakane and the Tsau faults, and in the Mababe Depression. The seismic activity is largely lower than in the Mid-Zambezi Rift with less than one earthquake per year since 1952 for magnitudes over 3 and a maximum magnitude of 6.7 measured in 1952 (Reeves, 1972a). The Makgadikgadi Basin presents sparse seismicity in its northern part and in the Makgadikgadi pans region whereas several earthquakes clustered in the southern part. A magnitude 6.5 earthquake affected this area in 2017. The focal mechanism suggests a NE dipping normal fault striking NW-SE almost orthogonal to the main trend of the MRZ and of the Okavango Graben (Kolawole et al., 2017; Mulabisana et al., 2021). Most of the seismicity in the Makgadikgadi Basin has been detected after 2004, leading some authors to suggest that a measurement bias resulted in underestimating the seismic activity in this region compared to others, such as the Okavango Graben (Nthaba et al., 2018; Pastier et al., 2017).

2.3. Geology of the Makgadikgadi-Okavango-Zambezi Basin

The basement of the MOZB consists of a series of Meso-to Neoproterozoic orogenic belts resulting from the collision of the Congo Craton to the northwest and the Kalahari Craton to the southeast (e.g., Haddon, 2005; Key & Ayres, 2000) (Figure 2b). The region was then affected by several extensional tectonic episodes between the Carboniferous and the late-Cenozoic: the Permo-Triassic Karoo rifting, a late Mesozoic-Cenozoic extensional episode and the Cenozoic still active EARS opening (Castaing, 1991; Van der Beek et al., 1998). During the Karoo rifting episode, detrital sedimentary series were deposited in the MOZB within NE-SW oriented grabens, as well as thick basaltic flows (e.g., Franchi et al., 2021; Jourdan et al., 2005). The MOZB is also cross-cut by a WNW-ESE dolerite dykes network aged of ∼179 Ma (Jourdan et al., 2004; Le Gall et al., 2002, 2005). During the Cenozoic, Southern Africa underwent a phase of erosion (e.g., Dauteuil et al., 2018; Guillocheau et al., 2018) and the African Superswell uplift, leading to the over 1,000 m.a.s.l. current elevations of the Southern African plateaus (Nyblade & Robinson, 1994). The whole area was then covered by fluvio-lacustrine and aeolian Kalahari

Figure 2. Geomorphology and geology of the MOZB. (a) Topographic map of the MOZB with main faults and geomorphologic features (modified after Eckardt et al., 2016; Moore et al., 2012; Pastier et al., 2017). Ch, Chobe; ChF, Chobe Fault; DeR, Deception Ridge; EG, Eiseb Graben; EK, Eastern Kalahari dune field; GdR, Gidikwe Ridge; GhR, Ghanzi Ridge; GuF, Gumare Fault; GwF, Gweta Fault; Hw, Hwange; KuF, Kunyere Fault; KuP, Kudiakam Pan; Li, Linyanti; LiF, Linyanti Fault; Ma, Mababe Depression; MaF, Mababe Fault; MaR, Magwikwe Ridge; MB, Makgadikgadi Basin; Mk, Makalamabedi Basin; MNS, Makgadikgadi Northern Shoreline; MRZ, Makgadikgadi Rift Zone; MZ, Mid-Zambezi Rift; Ng, Lake Ngami; NtP, Ntwetwe Pan; NxP, Nxai Pan; OD, Okavango Delta; OG, Okavango Graben; SuP, Sua Pan; ThF, Thamalakane Fault; TsF, Tsau Fault. Topographic data and symbology are similar to Figure 1. (b) Simplified geological map of the MOZB. Red annotations correspond to Precambrian belts and cratons from Pastier et al. (2017) (modified after Begg et al. (2009), Haddon (2005), Khoza et al. (2013), Kinabo et al. (2007), Miensopust et al. (2011), Muller et al. (2009), Singletary et al. (2003), and Youssof et al. (2013)). Karoo deposits are compiled from Jourdan et al. (2006), Key and Ayres (2000), and Wiles (1971). Kalahari deposits extent is from Haddon and McCarthy (2005). (c) Topographic profiles across the MOZB. Profile tracks are indicated in panel (a). Profiles are calculated over 20 km large envelopes with one profile line every 2 km and sampled every 100 m. Black lines correspond to the average values calculated over the envelope. Gray areas correspond to minimum and maximum values. A x500 vertical exaggeration is applied.

sediments, that deposited from the Late Cretaceous until today, with several phases of intra-basin erosion and sediment recycling (Haddon, 2005; Haddon & McCarthy, 2005) (Figure 2b). Desert conditions notably led to the formation of linear dune fields in the Kalahari Basin during the Late Neogene and Quaternary (e.g., Moore et al., 2012; Stone, 2021).

At the end of the Cenozoic and during the Quaternary, the MOZB hosted an extensive paleolake system, covering an area up to ~175,000 km^2 (Moore et al., 2012). On the basis of the different paleo-shorelines and gravel paleo-beaches, five major paleolakes of different water levels have been identified (Burrough et al., 2009; Cooke, 1979, 1980; Grey & Cooke, 1977; Grove, 1969; McFarlane & Eckardt, 2008; Moore et al., 2012; Podgorski et al., 2013; Riedel et al., 2014; Ringrose et al., 2005, 2009; Shaw, 1988): Paleolake Deception at 990–995 m above sea level (m.a.s.l.); Paleolake Makgadikgadi at 945 m.a.s.l. (Figure 2b); Paleolake Thamalakane at 936 m.a.s.l.; as well as two other unnamed paleolakes at 920 and 912 m.a.s.l. Their ages are poorly constrained and still debated, and two models diverge on their Quaternary history, as well summarized by Burrough et al. (2022). The Quiescent Model suggests a progressive desiccation of the paleolakes through the Pleistocene (e.g., Moore et al., 2012). In this model, the lakes would have contracted to a level under 936 m.a.s.l. before 500 ka. Time constraints are based on in-situ Early Stone Age (3 Ma to 300 ka) and Middle Stone Age (300–50 ka) artifacts found on the paleolake's beds as well as on phylogeographical evidences. Alternatively, the Dynamic Model proposes that the lakes experienced several episodes of drying and high-water level during the last 200 ka, with a last lacustrine episode at 945 m.a.s.l. occurring around 8.6 ka ago (Burrough et al., 2009). Time constraints are based on Optically Stimulated Luminescence (OSL) dating of paleo-shoreline sediments and stable isotope chronology on diatomites (e.g., Burrough et al., 2009; Cooke & Verstappen, 1984; Schmidt et al., 2017; Shaw, 1997). The establishment and regression of the paleolakes are alternatively interpreted as markers of climatic variations (Burrough et al., 2022) and as evolutions of the regional drainage network under tectonic constraints (Moore et al., 2012).

2.4. Geomorphology of the Makgadikgadi Basin

The Makgadikgadi Basin hosts the Makgadikgadi pans system (Cooke, 1980; Daly et al., 2020; Eckardt et al., 2008; Thomas & Shaw, 1991) and presents the lowest elevations of the MOZB and of the whole Kalahari Plateau, at around 890 m.a.s.l. in the southeast of the Sua Pan (Schmidt et al., 2017) (Figures 2a and 2c).

2.4.1. The Makgadikgadi Pans

Pans are vast flat areas whose soil consists of clays and silts, sometimes mixed and covered with evaporitic deposits, and sometimes indurated by calcretes and silcretes (Baillieul, 1979; Burrough et al., 2022; Franchi et al., 2020; Lancaster, 1978) (Figures 3a–3d). The Makgadikgadi Basin hosts the largest pan complex in southern Africa, of which the Ntwetwe Pan to the west and the Sua Pan to the east are the largest ones (Figure 2a). The processes of pan formation are not yet fully understood but wind deflation is recognized as the likely main driver (Burrough et al., 2022; Cooke, 1979; Lancaster, 1978). In the Makgadikgadi Basin it has been suggested that the pan formation also has a strong link with the lacustrine history of the basin (Franchi et al., 2020, 2022; Grey & Cooke, 1977; Haddon & McCarthy, 2005; Lancaster, 1978).

2.4.2. Lacustrine Paleo-Shorelines

Several lacustrine paleo-shorelines are observable over the Makgadikgadi Basin (Figure 2a). These paleo-shorelines are composed of multiple parallel sandy ridges identified as beach ridges following the Otvos (2000) definition, that is, "Relict, semi-parallel, multiple ridges, either of wave (berm ridge) or wind (multiple backshore foredune) origin" (Burrough et al., 2009; Cooke & Verstappen, 1984; Riedel et al., 2014; Thomas & Shaw, 1991). The Makgadikgadi Basin's beach ridges are mostly observable on east facing margins of the basin, suggesting prevailing easterly winds when they were deposited, similar to today (Burrough et al., 2009). The most prominent relic shoreline is the Gidikwe Ridge which forms a long sandy strip, peaking at around 940–950 m.a.s.l., concave toward the east and continuous for about 430 km along the western margin of the basin (Figures 2a and 2c). Its eastern face shows a series of parallel ridges made up of aeolian- and wave-accumulated sediments, matching the beach ridge description (Burrough et al., 2009; Grey & Cooke, 1977; Grove, 1969). Alternatively, the Gidikwe Ridge has also been interpreted as an offshore sandbar separated from the shoreline of the lake by a shallow lagoon (Cooke & Verstappen, 1984; Moore, 2013; Moore et al., 2012). In the northern part of the Makgadikgadi Basin, another Paleolake Makgadikgadi related shoreline extends from the south of the Nxai Pan to the west

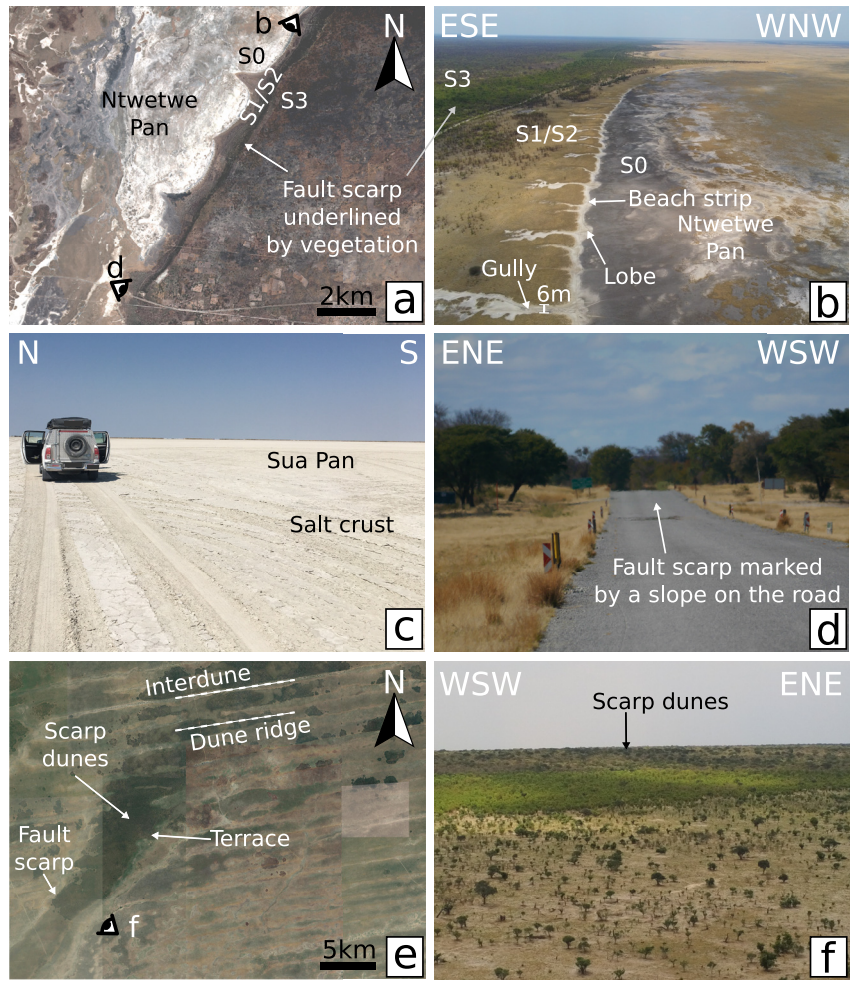

Figure 3. Pictures and satellite images of some geomorphological features in the Makgadikgadi Basin. (a) Satellite image of the Gweta Fault's scarp, forming the eastern margin of the northern part of the Ntwetwe Pan (© Copernicus Sentinel-2 data 2015). (b) Drone picture of the Gweta Fault's scarp. S0 to S3 annotations refer to surfaces described in the text. (c) Picture of the salt crust in the Sua Pan. (d) Picture of the Gweta Fault's scarp at the northeastern margin of the Ntwetwe Pan. (e) Satellite image of the linear dunes underlain by vegetation in the north of the Makgadikgadi Basin (Image © 2022 Maxar and Image © 2022 CNES/Airbus from Google Earth). (f) Drone picture of the front of scarp dunes. Eye symbols indicate the locations from which the pictures, referenced by figure numbers and letters, were taken.

of the Nata River Valley and has been far less studied than the Gidikwe Ridge (Eckardt et al., 2016; Ringrose et al., 2005). Given its location in the basin we will refer to this unnamed shoreline as the Makgadikgadi Northern Shoreline (Figures 2a and 2c).

2.4.3. Dunes

Several relict dunes have been described in and around the MOZB, belonging to the Mega-Kalahari sand sea (Grove, 1969). The predominant ones are linear dunes forming extensive dune fields sometimes covering several thousand square kilometers. These dunes are built parallel to a dominant wind, or to a resultant of two dominant winds, by accretion of eroded sand from the interdune and transport along the dune edge (Hollands et al., 2006; Lancaster, 1982; Livingstone, 1988; Tsoar et al., 2004). Among these dune fields, the Eastern Kalahari dune field is located in the Hwange area north of the Makgadikgadi Northern Shoreline (Stone, 2021; Thomas, 1984; Thomas & Burrough, 2016) (Figures 2a, 3e, and 3f). The Eastern Kalahari linear dunes trend E-W to ESE-WNW, are highly degraded and are covered with vegetation that outlines their track. They are currently 10–20 m high but were estimated around 60 m high when active (Grove, 1969; McFarlane & Eckardt, 2007; McFarlane et al., 2005). OSL dating indicates that they were already established at least in the Late Pleistocene (Ringrose et al., 2008; Stokes et al., 1997, 1998; Telfer & Thomas, 2007) and have undergone several periods of activity.

The last activity of the Eastern Kalahari linear dunes was dated around 20 ka, whereas activity has been recorded until 3–4 ka for other linear dunes located to the west of the Okavango Graben (Stokes et al., 1998; Thomas & Burrough, 2016). Close to fault scarps and drainage incisions, the eroded linear dunes locally show a more pronounced crest. It has been proposed that they are replicates of former flattened linear dunes, controlled by water infiltration (Eckardt et al., 2016; McFarlane & Eckardt, 2007). However, Jolivet et al. (2022) also showed that foredunes and parabolic dunes tended to form on downwind riverbanks in the Kalahari. They attributed their formation to perturbation of wind-flow in the vicinity of topographic obstacles such as river valleys and scarps. This process is not incompatible with the replicated dune model and should be considered regarding the importance of aeolian sand remobilization in the region (Garzanti et al., 2022; Telfer & Thomas, 2007). We will use the term "scarp dunes" to refer to dune morphologies that are related to topographic scarps. The aeolian system also includes lunette dunes forming on the downwind margin of pans and composed of sediments deflated from the pan floor during arid periods (Lancaster, 1978; Lawson & Thomas, 2002). Both linear and lunette dunes are markers of one or several arid episodes, necessarily drier than today and the time of paleolakes formation (McFarlane et al., 2005; Stokes et al., 1997; Thomas & Shaw, 1991). Their orientations suggest an E to ESE wind similar to the present-day direction.

2.4.4. Drainage Pattern

All rivers currently flowing into the Makgadikgadi Basin are intermittent (Figure 2a). The main ones are the Boteti River which flows out of the Okavango Delta and crosses the Gidikwe Ridge in the west, and the Nata River which flows into the Sua Pan in the northeast. The drainage systems to the south and north of the basin are fossil hydrographic systems (Shaw et al., 1992). The Makgadikgadi Basin is endorheic as no river exits from the basin.

2.4.5. Deformation of the Geomorphic Features

Several authors used the elevations of formerly presented geomorphological features to detect tectonic movements in the MOZB. Eckardt et al. (2016) studied the relationship between the Makgadikgadi Northern Shoreline, the linear dunes and the fault scarps in the north of the Makgadikgadi Basin. Based on topographic ridge elevation measurements, they described vertical displacements of Paleolake Makgadikgadi paleo-shorelines by tectonic movements subsequently to their formation. Gumbricht et al. (2001) suggested regional tilting based on elevation variations along the Gidikwe Ridge and the Magikwe Ridge (Figure 2a). However, these studies focused on the shorelines' highest ridges, which may in fact correspond to different geomorphological features that interact to form the topography of the shoreline (e.g., dunes, wave-built sandbars, erosive scarps). On the contrary, Burrough et al. (2009) suggested that tectonic movements had a minimal impact on the Makgadikgadi Basin's topography since the last lake highstand (8.6 ka ago according to them), based on the apparent consistency between shoreline elevations in the different MOZB's lacustrine sub-basins (Makgadikgadi Basin, Lake Ngami and Mababe Depression) (Figure 2a). They also highlighted that post-depositional processes such as erosion or dune reactivation complicate topographic interpretations and detection of neotectonic movements. Determining whether or not neotectonic movements occurred in the Makgadikgadi Basin since the last Paleolake Makgadikgadi highstand is however a major challenge for understanding the dynamics of the EARS in the MOZB as it may provide new chronological constraints on the rift propagation. Our work therefore seeks to better characterize the surface tectonic deformation based on a detailed geomorphological study of faults, dunes and paleo-shorelines.

3. Data and Methods

The geomorphological analysis of the Makgadikgadi Basin was carried out by (a) characterizing the morphology of fault scarps, dunes and paleo-shorelines in the field and (b) using a remote sensing approach to map these features at the Makgadikgadi Basin scale and to study their relationships. Two field campaigns were conducted in November 2021 and July 2022 in collaboration with the Okavango Research Institute (University of Botswana). Geomorphological observations were carried out on four key sites (Figure 4a): a 29 km-long section along the Gweta Fault scarp west of Zoroga village (GFS-1 field site), one site along the Gweta Fault scarp in the south of the Eastern Kalahari dune fields (GFS-2 field site), one site on the Gidikwe Ridge (GRS field site) and one site across the Makgadikgadi Northern Shoreline (NMS field site). Topographic profiles (Figures 4b–4d) were acquired with a Trimble® Geo7X receiver with a 20 min delay for phase alignment before recording each profile. The dual-frequency receptor with carrier phase filtered integrating the trajectory velocity enables to

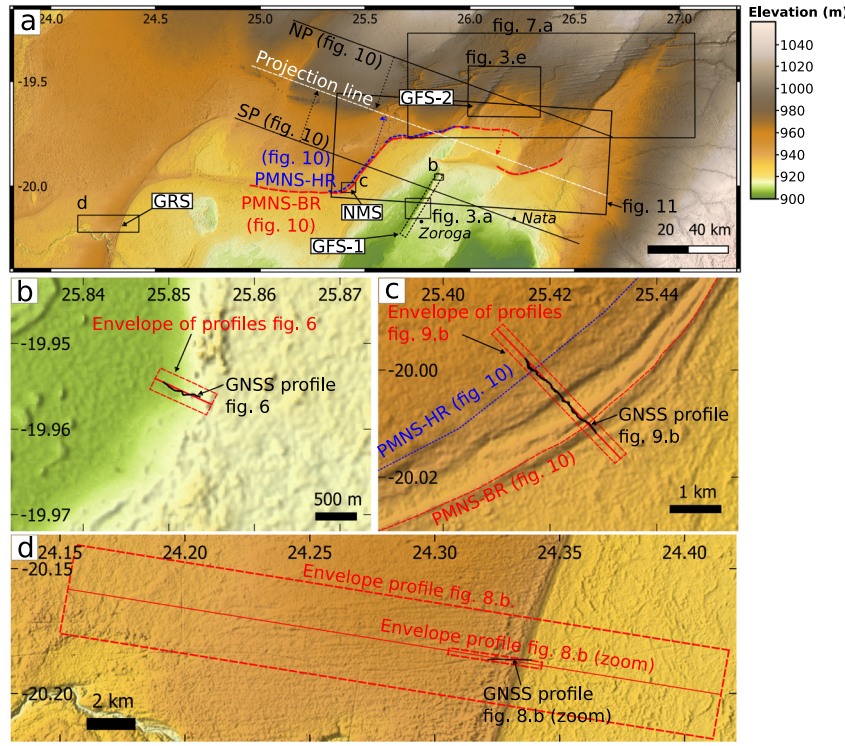

Figure 4. Field sites and topographic profiles localizations. White rectangles indicate field sites locations, black rectangles indicate figure locations. The location of panel (a) is given in Figures 2 and 5. Shaded topographic data: Copernicus GLO-30 DTED (ESA, 2019).

locally measure the topography of the geomorphological features with a <50 cm horizontal and a <1 m vertical relative accuracy (Kleusberg, 1986; Schwarz et al., 1989). The study area is remarkably flat with a ubiquitous aeolian sediment cover, so that most of the studied features have a discreet geomorphic expression on the field (Figures 3b, 3d, and 3f). Then, a remote-sensing approach was used to complete field observations. We used topographic data from the Copernicus GLO-30 DTED Digital Elevation Model (DEM), produced by the European Spatial Agency (ESA, 2019). It has a horizontal resolution of 1.0 arc-second in latitude (approximately 30.9 m) and 1.0 arc-second in longitude between latitudes 0° and 50° S (approximately 29 m in the area of the MOZB) for an absolute horizontal accuracy of less than 6 m. The absolute vertical accuracy is less than 4 m and the relative vertical accuracy fluctuates between less than 2 m and less than 4 m depending on the local slope (Fahrland et al., 2020). The DEM is not corrected for vegetation height, adding a potential bias on elevation measurements. Thus, geomorphologic interpretations were carried out preferentially with field data when available and the DEM was used to extend the analysis to the Makgadikgadi Basin scale. Most of the previous topographic studies in the MOZB used the 3 arc-second resolution Shuttle Radar Topography Mission (SRTM) elevation data (e.g., Eckardt et al., 2016). Thus, we compared the Copernicus and SRTM elevation data (USGS EROS, 2018) to detect potential elevation differences between these two data sets (Text S1, Figures S1 and S2 in Supporting Information S1). From the DEM, topographic profiles and elevation contours at different altitudes were extracted. In addition to the DEM, satellite images (Google Earth® and Sentinel-2 tiles) were used for mapping. Based on the field and remote sensing data we (a) mapped the lineaments and the fault scarps at the Makgadikgadi Basin scale, (b) characterized fault scarps morphologies, (c) analyzed the Eastern Kalahari dunes and interdunes' topography and (d) mapped the different geomorphological features composing the Paleolake Makgadikgadi shorelines and measured elevations along these features to evaluate their potential deformation.

Lineament mapping was conducted manually on DEM-derived topographic maps using multidirectional hillshade (illumination azimuths: 225°, 270°, 315°, 360°; illumination elevation: 45°; vertical exaggeration: x30) to mitigate biases associated with a single illumination source (Dauteuil, 1995; Scheiber et al., 2015; Smith & Clark, 2005). Following the definition of O'Leary et al. (1976), lineaments were defined as "mappable, simple or composite linear feature of a surface, whose parts are aligned in a rectilinear or slightly curvilinear relationship and which

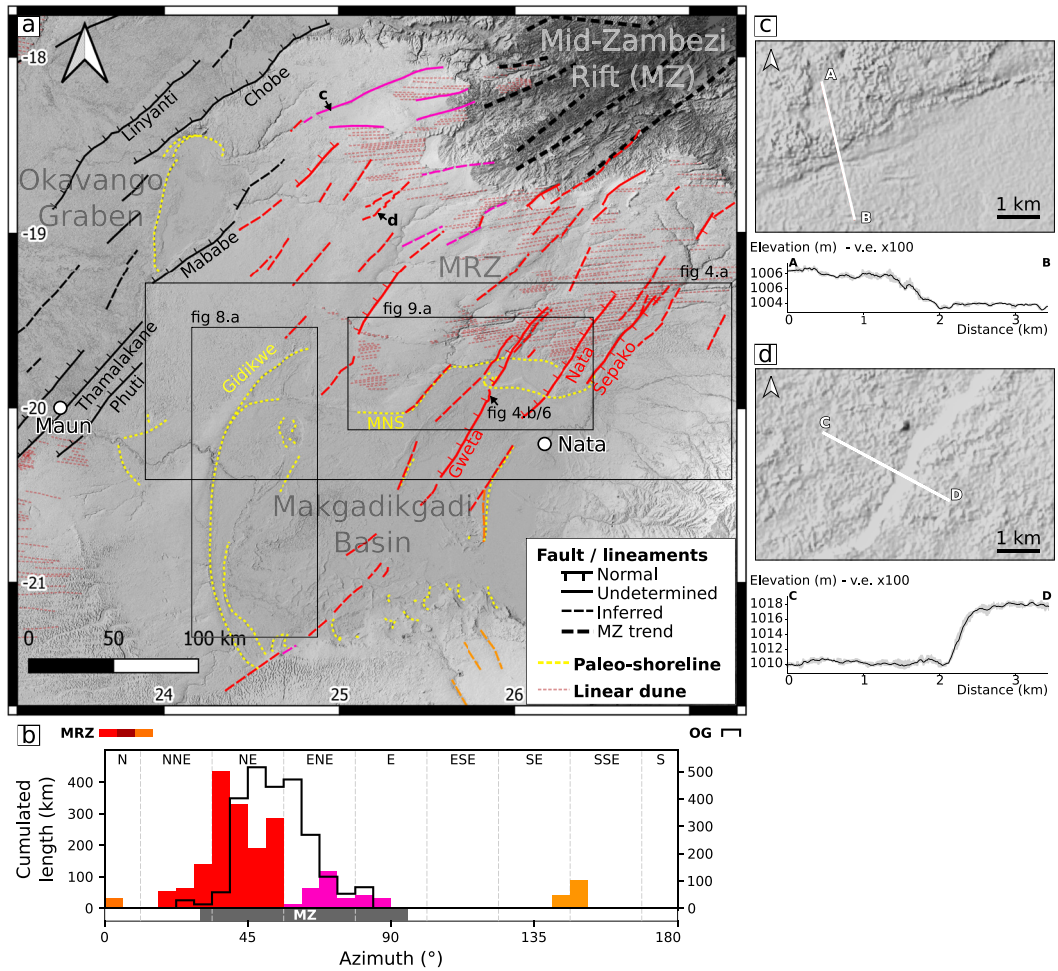

Figure 5. Map of the MRZ's faults and lineaments. (a) Red, magenta and orange lines correspond to the MRZ's faults and lineaments in accordance with directions presented on the bar graph shown in panel (b), thin black lines correspond to the Okavango Graben's faults and thick dashed black lines to fault trend in the Mid-Zambezi Rift. White dots correspond to main cities. The location is given in Figure 2. (b) The bar graph indicates the cumulated length of mapped fault scarps and lineaments as function of their azimuths. Colors corresponds to panel (a). Left-hand graduations correspond the MRZ's faults (red, magenta and orange colors) whereas right-hand graduations correspond to Okavango Graben's fault. The MZ gray bar represents the trending directions of faults in the Mid-Zambezi Rift. (c) Topographic map and profile of an ENE-WSW lineament. (d) Topographic map and profile of a NNE-SSW fault. v.e., vertical exaggeration. Shaded topographic background: Copernicus GLO-30 DTED (ESA, 2019).

differs distinctly from the patterns of adjacent features and presumably reflects a subsurface phenomenon," considering that they can be "continuous or discontinuous features" (Eckardt et al., 2016). We slightly deviated from O'Leary et al. (1976) by not presupposing subsurface relationships during mapping. Instead, topographic linear features were mapped and classified into categories: linear dune, suspected fault, shoreline related lineament, and unknown. Hydrographic lineaments have not been mapped except when they were aligned with suspected faults. Linear dunes and lacustrine shorelines in the MOZB have distinctive shapes that make them recognizable with remote sensing data (e.g., Eckardt et al., 2016; McFarlane & Eckardt, 2008; Moore et al., 2012; Riedel et al., 2014). The "suspected fault" class included lineaments exhibiting breaks in slopes delimiting topographic blocks and/or continuous features intersecting several lineaments from other classes. The final structural map retained: lineaments classified as suspected fault or unknown and lineaments from the other classes that are aligned with suspected faults in order to account for a potential tectonic control on the spatial layout of these features.

Fault scarp and shoreline morphologies were characterized using GNSS profiles, field observations and transverse composite profiles extracted from the Copernicus DEM. Additionally, longitudinal topographic profiles extracted from the Copernicus DEM along specific features of the shorelines aimed to identify lateral variations

in elevations. Longitudinal profiles were also extracted from the Copernicus DEM in the Eastern Kalahari linear dune field, both along dune ridges and interdunes. Profiles were compared to discriminate between topographic fluctuations related to dune construction/remobilization and break-in-slopes of the substratum.

4. Results

4.1. Fault Pattern of the Makgadikgadi Rift Zone

The surface expression of the faults affecting the Makgadikgadi Basin is characterized by linear scarps, contrasting with the surrounding flat topography. The structural map obtained from the remote sensing analysis shows a series of sub-parallel fault scarps and lineaments, with orientations ranging from NNE-SSW to ENE-WSW (Figures 5a and 5b). Outside the Okavango Graben, fault scarps and lineaments are observed from the northeast of the Mababe Depression to the northeast of the Nata Valley, mostly in the northern part of the Makgadikgadi Basin (Hwange area) (Figure 5a). This area is marked by a regional mean slope of less than 0.04°, dipping toward the Makgadikgadi pans to the south and toward the Okavango Graben to the west. The faults and lineaments cluster into three main groups depending on their trends (Figures 5a and 5b):

1. NNE-SSW to NE-SW trending faults (red features in Figures 5a and 5b) are dominant (80% of the total mapped fault length) and are observed throughout the Hwange area. This direction corresponds to that of the main faults in the Okavango Graben such as the Gumare and Thamalakane faults, but also to the trend of the Mid-Zambezi Rift (Figures 5a and 5b). Some of these faults extend southwards, where they delimit a topographic rise separating the Ntwetwe Pan from the Sua Pan. The topographic offsets along fault scarps then decrease in the pans, although some topographic lineaments may suggest that faults exist in the southern part of the pans.
2. The ENE-WSW to E-W trending lineaments (magenta features in Figures 5a and 5b) are less numerous (12% of the total mapped fault length) and found only in the northwestern portion of the Hwange area. They are close in direction to the boundary faults in the northeastern part of the Okavango Graben and in particular to the Chobe Fault, from which they are geographically close. Some of them display breaks in slope delimiting topographic compartments with different elevations (Figures 5c and 5d).
3. N-S to NW-SE trending lineaments (orange features in Figures 5a and 5b) suggest a third family of faults in the southern part of the Makgadikgadi Basin (8% of the total mapped fault length). However, no other evidence, such as offsets were found to confirm that they correspond to faults.

Regardless of their direction, faults and lineaments located in the northern part of the Makgadikgadi Basin are in continuity with the Mid-Zambezi Rift, where their traces on the DEM are lost in the rougher topography (Figure 5a). Lineaments with an ENE-WSW direction, located in the northwest of the Makgadikgadi Basin, establish a continuum with the Okavango Graben, pointing toward the Mababe Depression. Finally, the southwestern part of the Sua Pan, which is the lowest area of the MOZB, does not show any visible fault or lineament.

4.2. The Gweta Fault

The field survey at GFS-1 (Figures 4a and 4b) shows a ∼400 m wide and ∼8 m high scarp with a slope up to 2.5° (Figure 6a), to be compared with the regional slope of 0.04°. In the vicinity of this scarp, different depositional surfaces were identified, numbered S0 to S3 (Figure 6b). Surfaces S0, S1, and S2 are horizontal, lying downslope of the scarp and surface S3 constitutes the top of the scarp. The floor of the pan (S0) is composed of sandy clay and salt crusts and marked by desiccation cracks (Figure 6c). Between the pan and the scarp, the 40 cm to 1 m higher S1 surface is characterized by a sandy lithology covered with herbaceous vegetation. This surface is incised by small gullies over a depth of a few tens of centimeters and leading into the pan (Figure 6c). The limit between S0 and S1 is formed by a narrow sandy beach supporting small decimeter-thick sandy alluvial fans at the mouth of the gullies. Diatomite characterizing open-water lacustrine environments were also observed, intercalated between sandy layers and largely controlling the S2 surface (Figure 6c). The scarp itself forms a gentle slope covered with loose sand (Figure 6c). Due to the sandy cover, no fault plane was observed. At the top, the slope decreases until the surface becomes sub-horizontal (S3). The sandy cover of S3 contains loose silcrete and quartzite gravels and pebbles suggesting the proximity of the underlying basement (Figure 6c). Massive silcrete with green silcrete pebbles were also observed at a depth of 2 m in a small quarry at the top of the scarp. The surfaces were traced on the field for approximately 25 km along the scarp northwards from the A3 road, and it is likely that they continue for several tens of kilometers further north, as suggested by the DEM. To the south, the height of the scarp decreases until it disappears. Nonetheless, the continuation of the fault line can be inferred over several

10.1029/2023TC007988

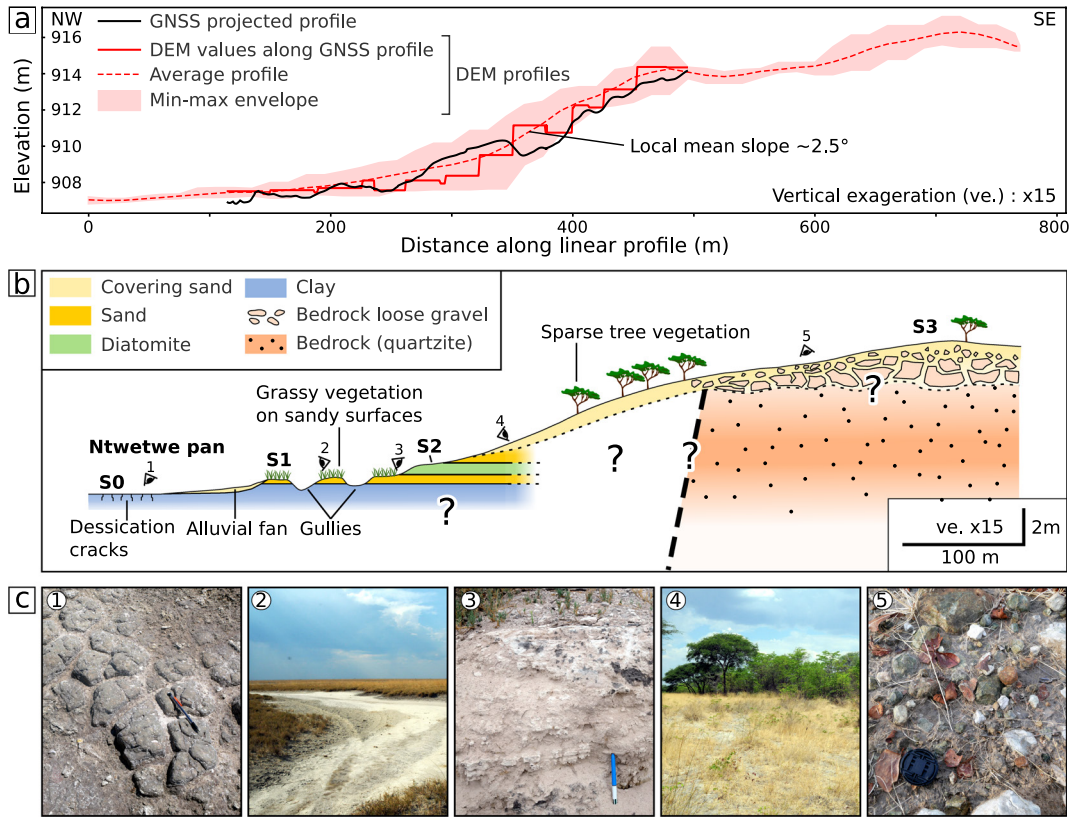

Figure 6. Topographic profiles across the Gweta Fault's scarp and interpretation. (a) Topographic profiles: black line corresponds to GNSS elevations obtained on the field and projected along the profile track; red lines and pink envelope correspond to Digital Elevation Model data. The localization of profiles is provided in Figure 4. (b) Geological interpretation of the topographic profiles based on geomorphological and sedimentological observations made in the field. Eye symbols indicate the position and orientation of pictures shown in panel (c). (c) Pictures of the different lithologies observed around the Gweta Fault scarp and used to establish the geological cross section: (1) Desiccation cracks in the dark and salted clay layer forming the bottom of the ephemeral lake; (2) Fine-grained white sandy layer deposited on the dark clay and forming both isolated buttes and the present-day shore of the lake; (3) Meter-thick diatomite layer interbedded between two fine-grained sandy layers. These layers are exposed laterally in warthog holes dug along the shoreline upper surface; (4) Aeolian sand covering the surface or the fault scarp; (5) Pebbles and cobbles of silcrete and metamorphic basement associated with some larger outcrops of silcrete indicating the presence of bedrock below a thin layer of clastic debris.

kilometers from the morphology of the Ntwetwe Pan on the DEM and the alignment of the vegetation observed on satellite imagery (Figures 3a and 3b), until it fades completely within the Ntwetwe Pan.

Field investigations conducted at the GFS-2 site (Figures 4a, 7a, and 7b) show a totally different landscape where none of the surfaces described at GFS-1 were recognized. The area investigated corresponds to a sandy valley with clayish waterholes. Remote sensing data show a ~300 m wide surface with an approximate 1.0° slope toward the WNW located on the eastern side of the valley (Figure 7b). This scarp is in continuity with the Gweta Fault scarp described at GFS-1. Remote sensing data show that the fault scarp intersects linear dunes. No horizontal offset of the linear dunes has been detected but topographic profiles along the dunes' ridges and interdunes show a 4 m vertical offset (Figure 7c).

The vertical offset of the basement deduced from the geological cross-section at GFS-1 and the orientation of the slope of the scarp indicate a northwest-directed normal component on the Gweta Fault (Figure 6b). Furthermore, the lack of lateral offset of the dunes' axis around GFS-2 suggests that the fault is mainly normal-dip.

4.3. Topography of the Eastern Kalahari Dune Field

Linear dunes south of the Eastern Kalahari dune field can be followed almost continuously on the DEM on more than 150 km for some of them, with a constant ENE-WSW (~N 080°) direction. Linear dunes intersect several

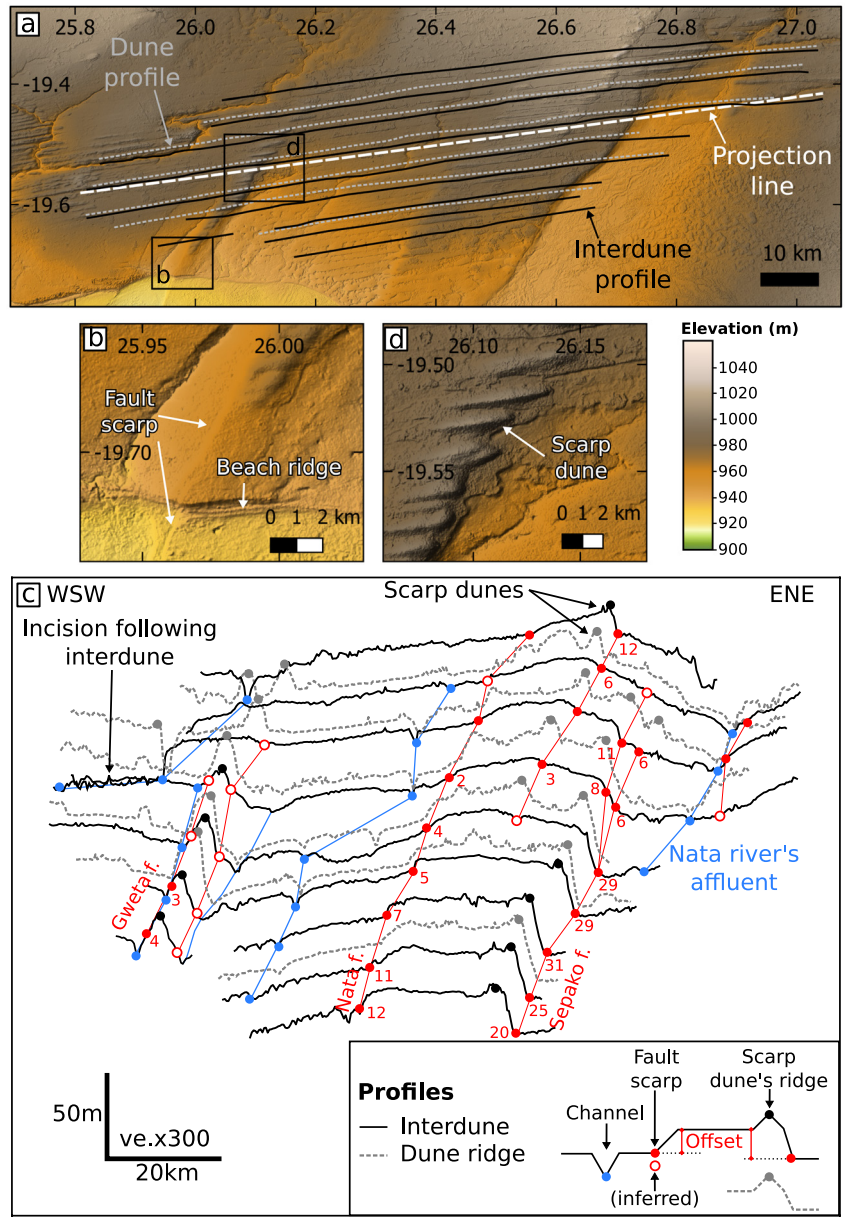

Figure 7. Geomorphology of the Eastern Kalahari linear dune field. (a) Digital Elevation Model (DEM) view of the Eastern Kalahari dune field with the location of the profiles tracks of panel (c). (b) DEM view of a portion of the Gweta Fault intersecting the Eastern Kalahari linear dunes and the Makgadikgadi Northern Shoreline. (c) Projected topographic profiles along the Eastern Kalahari linear dunes ridges and interdunes. Profiles are not at the same elevation of origin (they are offset vertically one to each other) but they have the same scale with a x300 vertical exaggeration (ve). Lower profiles are the southern profiles and upper profiles are the northern profiles. All profiles were projected horizontally on a same projection line. Blue lines correlate incisions (blue dots) pointed on interdunes' profiles. Red lines correlate fault scarps (red dots) pointed on interdune profiles. Red numbers indicate topographic offsets measured at fault scarps (in meter). Black and gray dots indicate scarp dunes' summits along interdunes and dune ridges profiles respectively. Profile tracks are given on panel (a). (d) DEM view of scarp dunes.

of the fault scarps without observable horizontal offset (Figure 7a). Linear dune ridges, and few interdunes, are capped with scarp dunes where they are intersected by east-facing, NNE-SSW trending fault scarps (Figures 7c and 7d). Topographic profiles obtained from DEM data along interdunes and dune ridges show vertical topographic offsets correlated to fault scarps (Figure 7c). In order to minimize measurement uncertainties due to the scarp dunes, only interdunes are considered showing up to 31 m of vertical offsets. The highest offsets are measured along the Sepako Fault at the western margin of the Nata Valley, but they must be considered carefully

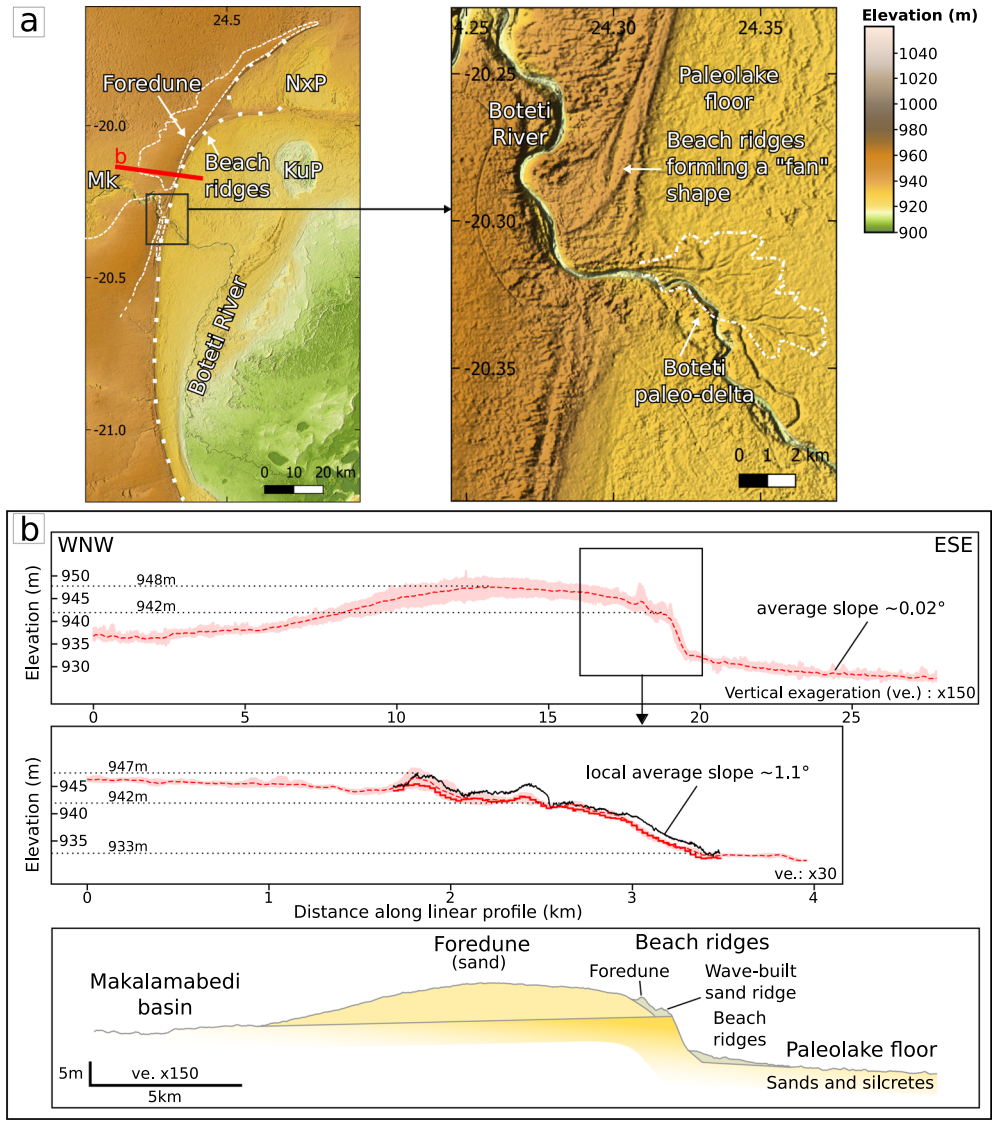

Figure 8. Geomorphology of the Gidikwe Ridge. (a) Digital Elevation Model (DEM) view of the Gidikwe Ridge with a focus on a segment of the Gidikwe Ridge at the outlet of the Boteti River showing fan shaped beach ridges and a paleo-delta. Dashed white lines indicate foredunes contour, thick dotted lines indicate beach ridges and dashed and dotted white lines indicate the Boteti paleo-delta. The red line indicates the position of profiles of panel (b). Location of panel (a) is given in Figure 5. KuP, Kudiakam Pan; Mk, Makalamabedi Basin; NxP, Nxai Pan. (b) Topographic profiles across the Gidikwe Ridge with field observations and interpretations. The black line corresponds to a GNSS profile carried out at GRS field site. Red lines and envelopes correspond to profiles extracted from the DEM (see Figure 6a for legend). Profile tracks are given in Figure 4d.

as offsets might have been accentuated by the incision of the Nata River. Several fault scarps observable in the Eastern Kalahari dune field can be followed continuously southward, in the pans area and show intersections with lacustrine shorelines (e.g., Gweta Fault and Nata Fault; Figures 5a and 7b).

4.4. Lacustrine Shorelines Morphology

4.4.1. The Gidikwe Ridge

Remote sensing data show that the Gidikwe Ridge extends from the southwestern corner of the Ntwetwe Pan toward the north of the Nxai Pan (Figure 8a). At first order, the Gidikwe Ridge has a short face to the east and a long face to the west. Between the Nxai Pan and the Kudiakam Pan, the ridge splits in two, with a branch joining

the Makgadikgadi Northern Shoreline toward the east and another one continuing toward the northeast, parallel to the western margin of the Nxai Pan (Figure 8a). The Gidikwe Ridge is continuous along its entire length, except at the level of the Boteti River which cuts into it.

The GNSS topographic profile performed at the GRS site shows a series of four successive ridges 1–3 m high and 150–360 m wide, capping the top of a ∼1.1° sloped scarp facing to the east (Figure 8b). The ridges peak at an elevation ranging between 947 m.a.s.l. for the western one and 942 m.a.s.l. for the eastern ones. The following geomorphological features were identified on the Gidikwe Ridge, from east to west, based on correlations between field observations and the remote sensing analysis (Figures 8a and 8b):

1. The lake-bed. Downslope to the east of the Gidikwe Ridge is a flat surface with a ∼0.02° slope leaning toward the Ntwetwe Pan. This surface is interrupted to the east by the western margin of the Ntwetwe Pan, which also displays a series of sand ridges located between 930 and 910 m.a.s.l. Silcretes and sandy deposits have been observed here, although no detailed mapping has been carried out. This surface is remarkably smooth on the DEM except where the Nxai Pan and Kudiakam Pan form distinct topographic depressions (Figure 8a), which themselves display series of ridges on their western margins. The surface is also incised by channels coming from the Gidikwe Ridge, including the present-day channel of the Boteti River. Where the Boteti River flows out of the Gidikwe Ridge, the DEM shows small abandoned diverging channels forming a paleo-delta (Figure 8a).
2. Beach ridges. The eastern base of the Gidikwe Ridge is marked by a sharp break in slope followed by a series of small ridges. These ridges are composed of sand, sometimes locally cemented (incipient silcrete and calcrete), and can be followed almost all along the Gidikwe Ridge on the DEM (Figure 8a). They are only interrupted in the northern part of the Gidikwe Ridge and where the Gidikwe ridge is intersected by the drainage system. At the mouth of the Boteti River in the Makgadikgadi Basin, the sand ridges get spaced out forming a fan-shape on both sides of the river (Figure 8a). This disposition of the sand ridges suggests that the Boteti River had an influence on the deposition of the beach ridges implying that the river was flowing into the Paleolake Makgadikgadi during lacustrine episodes, which is also supported by the presence of the paleo-delta.
3. Bypass surface. Behind the sandbars, the Gidikwe Ridge displays a gently sloping area facing east, forming a surface of several hundred meters to several kilometers wide, locally incised by the recent drainage system.
4. Foredune. The western part of the Gidikwe ridge has a dome-shaped topography, with a short steep east-facing face and a longer west-facing face, culminating at an altitude of between 950 and 960 m.a.s.l. (Figure 8b). This morphology corresponds to a dune system that runs the length of the Gidikwe Ridge, although it is less marked in its southern part. The dune system is incised by the drainage system and by small pans up to 2–3 km in diameter, with sand ridges on their western edge.
5. Lagoon-like depression. West of the Gidikwe Ridge, the topography locally displays elevations lower than the beach ridges, such as in the Makalamabedi Basin (Figures 8a and 8b). These low areas are thus currently below the paleolake level associated with the beach ridges. These low elevation areas located behind the sand ridges suggest the presence of lagoons, assuming that these low elevations already existed during the lacustrine episode. The low elevations behind the Gidikwe Ridge could also result from erosion post-dating the lake, such as wind deflation.

4.4.2. The Makgadikgadi Northern Shoreline

Field survey at the NMS site (Figures 9a and 9b) shows, from southeast to northwest, a series of parallel ridges approximately 1–6 m high and 190–310 m wide, culminating between 937 and 942 m.a.s.l. They are followed by a ∼400 m wide depression at the foot of a 6 m high scarp. The top of the scarp is characterized by a 600 m wide flat surface after which the topography rises up to over 950 m.a.s.l. forming a dome shape. The same geomorphological features as on the Gidikwe Ridge were identified along the Makgadikgadi Northern Shoreline (Figures 9a and 9b). Additionally, topographic depressions locally suggest the existence of lagoons between the beach ridges and the dunes. On remote sensing data, dunes and bypass surfaces were only identified along the east and southeast facing portions of the Makgadikgadi Northern Shoreline (Figures 9a and 9b). Beach ridges are observed almost continuously along the entire length of the Makgadikgadi Northern Shoreline except where the shoreline intersects the drainage system. The DEM shows that the Makgadikgadi Northern Shoreline has a sinuous track affected by several sharp turns (Figure 9a). The turns separate the shoreline into segments with two main directions: some have a direction fluctuating between ESE-WNW and ENE-WSW, while others have a

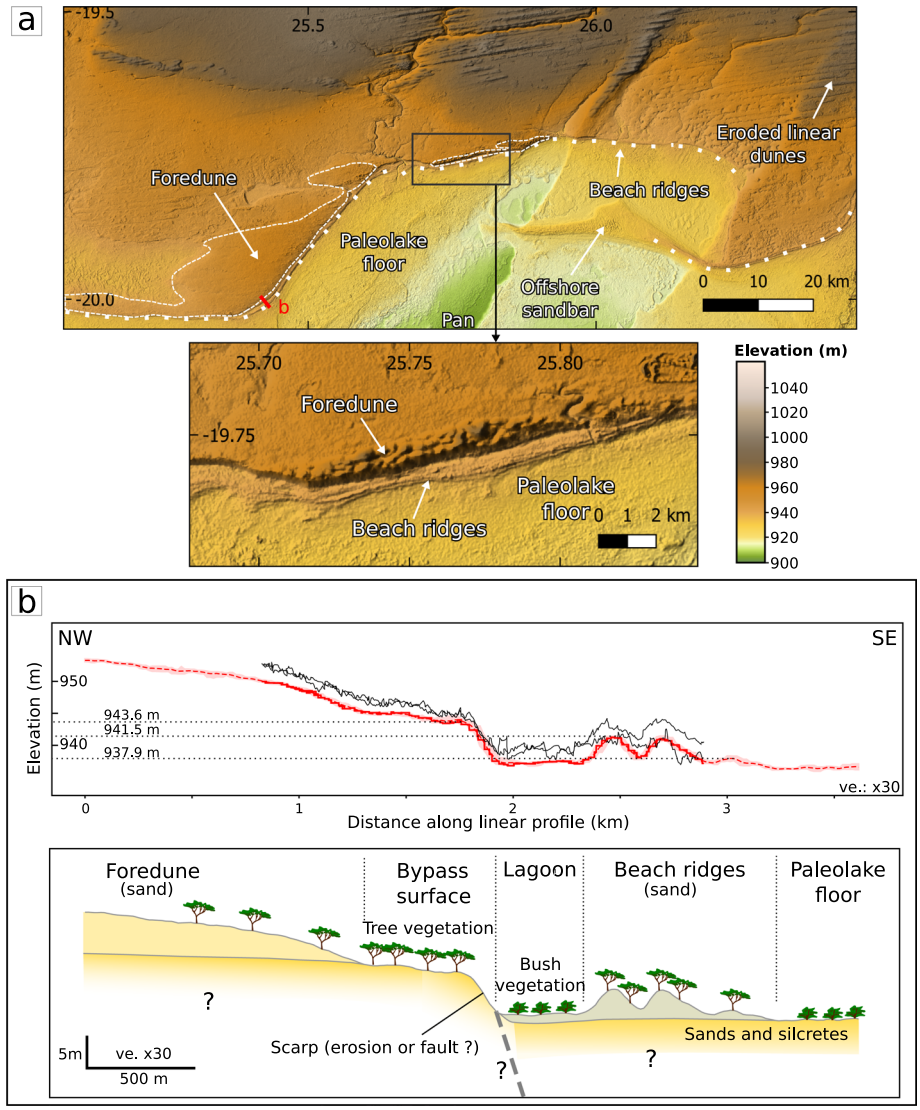

Figure 9. Geomorphology of the Makgadikgadi Northern Shoreline. (a) Digital Elevation Model (DEM) view of the Makgadikgadi Northern Shoreline with a focus on beach ridges and foredunes. Dashed white lines indicate foredune contours and thick dotted lines indicate beach ridges. The red line indicates the position of profiles of panel (b). Location of panel (a) is given in Figure 5. (b) Topographic profile across the Makgadikgadi Northern Shoreline with field observations and interpretations. Black lines correspond to GNSS profiles carried out at NMS field site. Red lines and envelopes correspond to profiles extracted from the DEM (see Figure 6a for legend). Profile tracks are given in Figure 4c.

rectilinear NNE-SSW direction. Finally, all along its track, the Makgadikgadi Northern Shoreline delineates the very smooth surface of the paleolake floor to the south, from the more rugged topography of the land area to the north, marked by the presence of linear dunes and river incisions (Figure 9a).

4.4.3. Elevation of Shorelines

Measurements taken on the DEM along a continuous beach ridge along the Gidikwe Ridge and the Makgadikgadi Northern Shoreline show an almost constant elevation of around 941 m.a.s.l. (Figure 10). However, at the western tip of the Makgadikgadi Northern Shoreline, between the Nxai Pan and the Kudiakam Pan (Figure 2a), the elevation of the sand ridge gradually decreases toward the west, from 941 to 935 m.a.s.l. This progressive and localized variation in elevation is probably of sedimentary origin given the parallel orientation of this section of the shoreline to the main wind direction. The beach ridges are continuous, even at the level of fault escarpments, where they do not show vertical or horizontal offsets. The almost constant elevation of the beach ridges contrasts with the surrounding piano-key topography and with the topographic profile following the highest

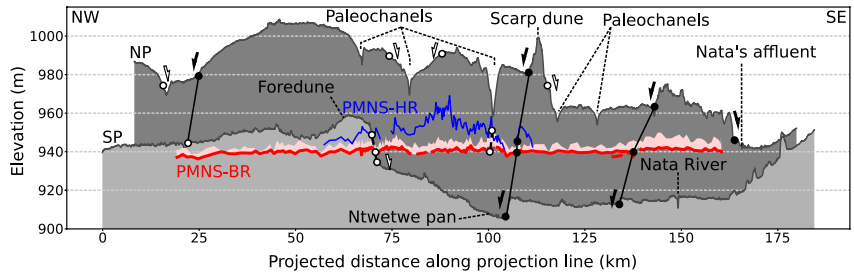

Figure 10. Topographic profiles of the Makgadikgadi Northern Shoreline and the northern Makgadikgadi Basin extracted from Copernicus Digital Elevation Model (DEM). Red line (PMNS-BR) corresponds to a longitudinal profile along a beach ridge; light-red area corresponds to the difference between elevation measured on the Copernicus DEM and the Shuttle Radar Topography Mission elevation data along the beach ridge; blue line (PMNS-HR) corresponds to a longitudinal profile along the highest ridge of the shoreline (when identified); dark gray (NP) and light gray (SP) profiles correspond to straight profiles in the northern Makgadikgadi Basin. Black dots and white dots indicate where profiles intersect faults and inferred faults respectively. Black lines link dots corresponding to the same faults. Black arrows indicate dips of faults, white arrows indicate inferred dips of inferred faults. Profile tracks are given in Figure 4a. All profiles are projected along a straight projection line (Figure 4a).

points along the shoreline. Indeed, the latest shows a fluctuating elevation ranging between 940 m.a.s.l. and 965 m.a.s.l. (Figure 10).

5. Discussion

5.1. Deformation in the Makgadikgadi Rift Zone

The fault pattern of the MRZ (Figure 5) obtained through this study is coherent with the one proposed by Eckardt et al. (2016), showing a staircase structure affecting the northern part of the Makgadikgadi Basin (Figures 10 and 11). The vertical offsets measured along the Eastern Kalahari interdunes and the lack of horizontal displacements suggest pure extension in the northern part of the MRZ (Figures 7a and 7c). The vertical topographic offset values obtained must however be considered carefully to estimate fault throws as they may have been impacted by erosive and depositional processes (e.g., incision and/or alluvial deposits in the Nata River Valley). The MRZ fault scarps fade out in the Makgadikgadi pans, where the number of lineaments decreases from north to south. Two hypotheses can be put forward. First, the faults might end by buffering in the pans. Second, the fault scarps might have been erased by erosion and/or sedimentation, as suggested by the occurrence of some linear structures in the south of Ntwetwe Pan. This second option has to be considered regarding the sequence of development of the pans which alternates between phases of erosion (mostly wind-deflation) and shallow lacustrine sedimentation (Lancaster, 1978). It would then imply that these fault portions have been inactive at least since the last phase of erosion and/or sedimentation. Whether the faults continue through the Makgadikgadi pans or not, they are absent from the region south of the Makgadikgadi Basin and end at the southern margin of the pans or before. The lowest elevations of the Makgadikgadi Basin are in its southeastern part, where no lineament has been detected, while the northwestern highest part of the basin is affected by faults with significant throws (over 10 m). These observations suggest that the topographic depression of the Makgadikgadi Basin does not result from tectonic activity. Unlike the Okavango Graben, whose current shape results from EARS-linked deformation (e.g., Modisi, 2000), the Makgadikgadi Basin is likely not an EARS-related tectonic depression and another process independent from the EARS generated it.

5.2. Relative Chronology of the Makgadikgadi Rift Zone

The remote sensing topographic measurements along the Gidikwe Ridge and the Makgadikgadi Northern Shoreline show a constant elevation of the summit of one of the sand ridges at around 941 m.a.s.l. Its constant elevation and near continuity make it a good landmark all-along the different segments of the shoreline, consistent with a beach ridge feature. Moreover, the shape of the sandbar where the Boteti River crosses the Gidikwe Ridge (Figure 8a) shows that the sandbar was located at the level of the river outlet in the lake. This beach ridge is thus a reliable marker of the level of the lake. The 941 m.a.s.l. elevation is consistent with the 945 m.a.s.l. usually attributed to the Paleolake Makgadikgadi considering the absolute elevation variations that can exist between

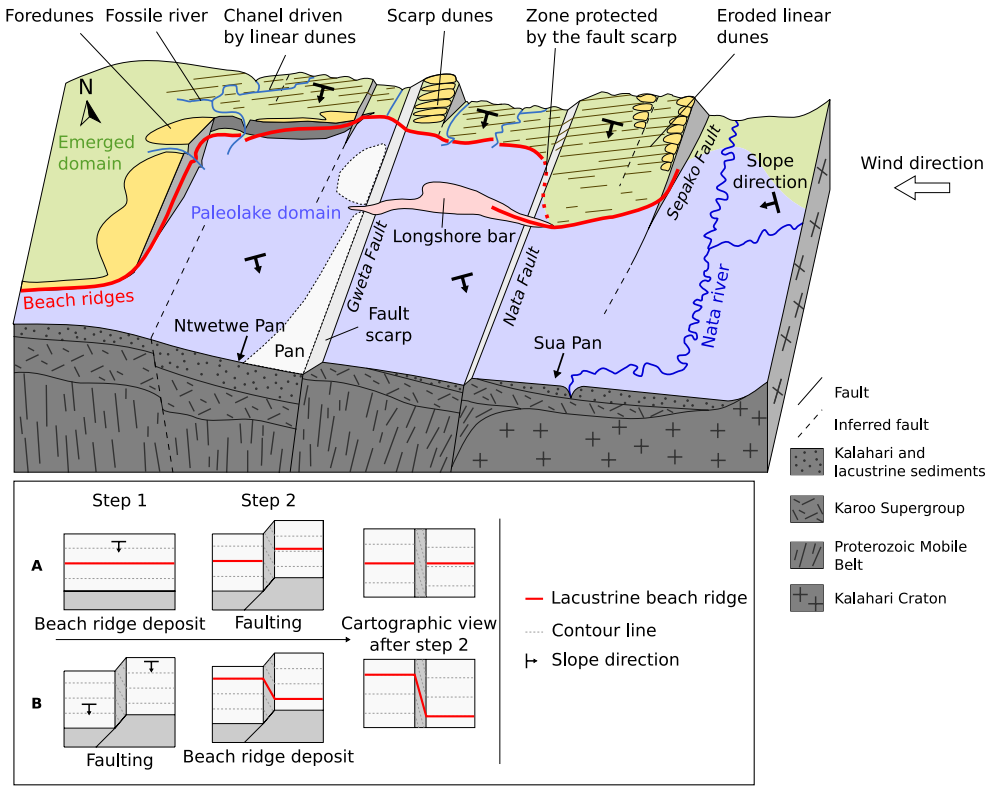

Figure 11. Synthetic 3D block of the geology and geomorphology of the northern Makgadikgadi Basin. The scale is not respected. At the bottom, scenarios A and B show the theoretical final morphology of a sand ridge based on the relative timing between normal faulting and sand deposition in a sloping area. The morphology of the beach ridges of the Makgadikgadi Northern Shoreline is consistent with scenario B. The approximate location of the synthetic 3D block is given in Figure 4a.

the different DEM data sets (Text S1 in Supporting Information S1). In the MOZB, elevations given by the Copernicus DEM are on average 3.2 m lower than those given by the SRTM data (Text S1, Figures S1, and S2 in Supporting Information S1). The position of the 941 m.a.s.l. beach ridges implies that the Gidikwe Ridge, which peaks at >950 m.a.s.l., was above the water level when the beach ridges formed. These observations contradict former interpretations of the Gidikwe Ridge as an offshore sandbar (Cooke & Verstappen, 1984; Moore, 2013; Moore et al., 2012). However, the possibility of previous lacustrine stages characterized by higher lake levels corresponding to the interpretation of the Gidikwe Ridge as an offshore sandbar is not excluded.

Elevations measured along the beach ridge remain constant even when it is intersected by fault scarps. These constant elevations suggest that the beach ridge underwent no or very little deformation and post-depositional erosion since its formation. This result contradicts the conclusion of Gumbricht et al. (2001) and Eckardt et al. (2016) who proposed that neotectonic movements tilted the Gidikwe Ridge and deformed the Makgadikgadi Northern Shoreline respectively. We identified two potential bias in these studies. Gumbricht et al. (2001) produced one of the first topographic maps of the region by interpolating spot elevation measurements with most data spaced at around 7.8 km each, which is too imprecise to detect the different geomorphological features that compose the shorelines. Eckardt et al. (2016) used the 3 arc-second resolution SRTM data that have a lower resolution than the Copernicus DEM and took as reference the highest elevations around the effective shoreline: our detailed analysis shows that shorelines are composed of several geomorphological features such as dunes, erosional scarps or wave-built sandbars (Figures 8, 9, and Figure S2 in Supporting Information S1). Elevations along the shoreline can be correlated only if they are measured on a same sedimentary feature. Elevations along dunes depend on several factors such as wind exposure or sand availability and erosional scarps elevation can reflect a relict topography, so they are unreliable markers. In contrast, wave-built beach ridges' elevations are constrained by the lake levels and remain laterally constant if not deformed. In that way, the 941 m.a.s.l. constant elevation of the studied sandbar suggests that the main tectonic activity of the MRZ pre-dated the lake that

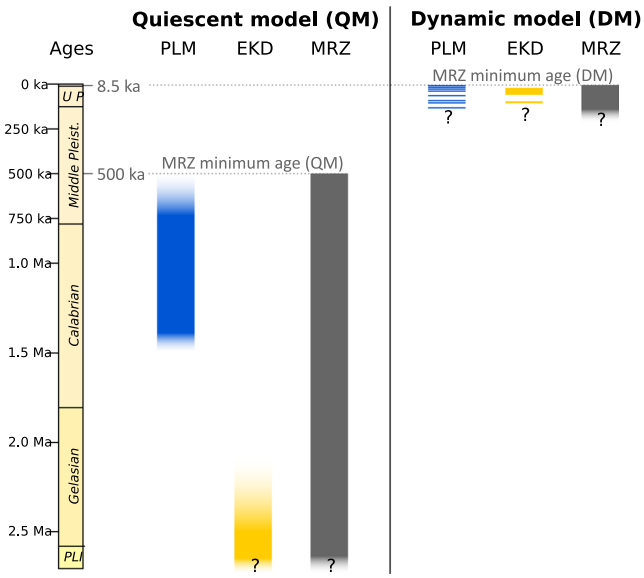

Figure 12. Constraints on the relative chronology of the Makgadikgadi Rift Zone (MRZ) based on two different models from the literature. PLM, Paleolake Makgadikgadi; EKD, Eastern Kalahari linear Dunes; MRZ, Makgadikgadi Rift Zone. For the Quiescent model (QM) ages are from Moore et al. (2012). For the Dynamic model (DM) ages are from Burrough et al. (2009) and Thomas and Burrough (2016). MRZ ages are deducted from PLM and EKD ages (see text). PLI, Pliocene; UP, Upper Pleistocene.

generated the sandbar. Another argument for the fault scarps to predate the sandbar is the sinuous geometry of the beach ridges on the map (Figure 11). The NNE-SSW segments of the Makgadikgadi Northern Shoreline fit perfectly with the fault scarps direction and some segments of the shoreline directly follow some fault scarps. This correlation between fault and local shoreline directions suggests that the NNE-WSW segments of the Makgadikgadi Northern Shoreline followed existing fault scarps (Figure 11).

The remote sensing analysis shows that the Eastern Kalahari linear dunes are interrupted to the south by the Makgadikgadi Northern Shoreline and are totally absent from the Paleolake Makgadikgadi floor area, clearly proving they are older than the Makgadikgadi Northern Shoreline. Offsets measured along interdunes and dune ridges where they intersect fault scarps show that they have been deformed by the tectonic activity in the MRZ. Apart from these vertical offsets, linear dunes remain remarkably continuous and parallel all over the Eastern Kalahari dune field, even when intersected by fault scarps. The linear dunes thus formed on a smooth substratum free of fault scarps that would have disturbed sand accumulation in their vicinity. All these arguments suggest that the Eastern Kalahari linear dunes are older than the activity of the MRZ's faults.

Based on these observations, the following relative chronology is proposed: (a) the Eastern Kalahari linear dunes formed on a tectonically stable substratum, (b) the Makgadikgadi Basin was then affected by NNE-SSW to E-W extensional faults, (c) fault activity decreased and (d) the basin was flooded during a humid period forming a vast lake with a surface elevation of around 941 m.a.s.l. (Paleolake Makgadikgadi). Finally, (e) changes in the hydrological regime induced by increased aridity (Burrough et al., 2022) and/or reorganization of the drainage system (e.g., Moore et al., 2012) led to the drying up of the paleolakes. The proposed relative chronology is not exhaustive: other lacustrine episodes of higher or lower levels could have occurred between steps (a), (b), (c) and (d). Step (d) only represents the last lacustrine episode that reached the ~941 m.a.s.l. level, possibly erasing the features built by previous, lower altitude flooding episodes.

Given the established relative chronology, absolute ages on the onset of Eastern Kalahari linear dunes formation would constrain a maximum age for the initiation of MRZ activity whereas ages on the last Paleolake Makgadikgadi beach ridges would constrain a minimum age for the end of the main tectonic activity of the MRZ. Several ages have been proposed in the literature, both for the Paleolake Makgadikgadi Shorelines and the linear dunes, and as previously indicated, two models are currently debated (Burrough et al., 2022) (Figure 12). The Quiescent Model implies that the last Makgadikgadi lake with a 941 m.a.s.l. level dried up to a lower level before 500 ka and that the Eastern Kalahari linear dunes have an Early Pleistocene minimum age (McFarlane et al., 2005; Miller et al., 2010; Moore et al., 2012). Given the proposed relative chronology presented in this study, the Quiescent Model would imply that the activity of the MRZ decreased before the Middle-Pleistocene but does not delimit a maximum age for the onset of MRZ formation. On the other hand, according to the Dynamic Model, the younger OSL ages measured on the Gidikwe Ridge is 8.6 ± 0.9 ka (Burrough et al., 2009; note that the drill site's coordinates given in Burrough et al. (2009) correspond to the 941 m.a.s.l. undeformed beach ridge we focused on in this work). Given the proposed relative chronology presented in this study, the Dynamic Model would imply that the MRZ remained inactive or poorly active since early Holocene. Existing OSL ages on Eastern Kalahari linear dunes span from <20 to 115 ka but do not exclude older dunes' construction phases (Stokes et al., 1997), so they do not constrain a maximum age for the MRZ activity. Thus, existing data do not allow for precisely constraining the age of the activity of the MRZ. However, the ages from literature support that the MRZ has remained poorly active at least since 8.6 ka, if we consider the most conservative minimum age of the two models.

5.3. Propagation of the East African Rift System in the Makgadikgadi-Okavango-Zambezi Basin

The lineaments and faults pattern obtained from the DEM analysis shows that the NNE-SSW faults of the MRZ are in continuity with the Mid-Zambezi Rift (Figures 5a and 13). As a consequence, the MRZ represents the end

10.1029/2023TC007988

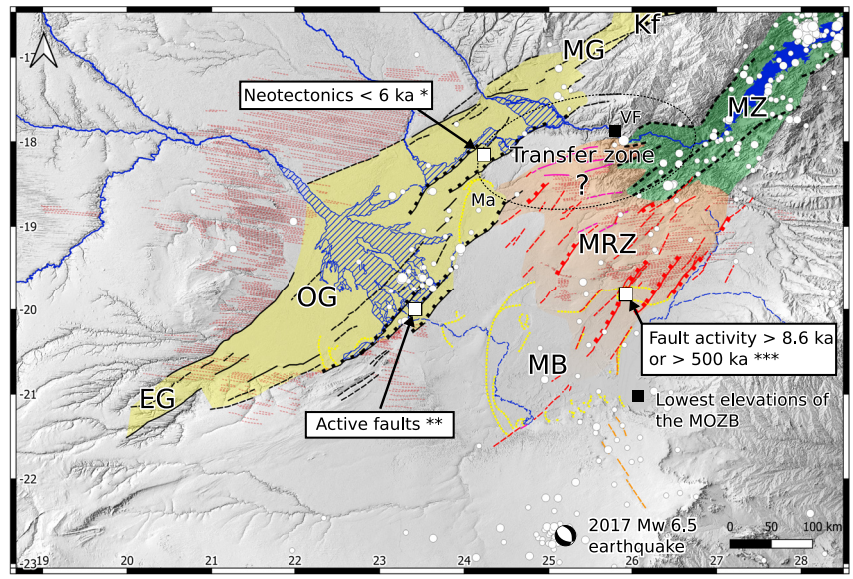

Figure 13. Synthesis of the EARS dynamics in the MOZB. EG, Eizeb Graben; Kf, Kafue Graben; Ma, Mababe Depression; MB, Makgadikgadi Basin; MG, Machili Graben; MRZ, Makgadikgadi Rift Zone; MZ, Mid-Zambezi Rift; OG, Okavango Graben; VF, Victoria Falls. Legends: earthquakes cf., Figure 1, geomorphic features cf., Figure 2, faults cf., Figure 5. Colored areas correspond to zones of EARS induced deformation. The question mark indicates that the transfer zone is hypothetical. * Mokatse et al. (2022); ** Bufford et al. (2012); *** this study.

of a corridor of the Southwestern Branch of the EARS, going through the Mid-Zambezi Rift, as proposed by Daly et al. (2020) (Figure 1b). The normal-dip kinematic and the NNE-SSW to NE-SW strike of the MRZ faults suggest that the MRZ formed under a general WNW-ESE to NW-SE extension.

NE-SW to E-W lineaments in the northwestern part of the MRZ also link the Mid-Zambezi Rift to the Okavango Graben. Eckardt et al. (2016) recognized these lineaments on geomagnetic data and DEM, and interpreted them as faults. Some of the NE-SW lineaments form topographic offsets but of much lower amplitudes than the NNE-SSW ones (Figures 5c and 5d). More arguments are needed to confirm their tectonic origin, but if attested, they would draw a corridor of deformation between the Mid-Zambezi Rift and the Okavango Graben (Figure 13).

The staircase topography of the MRZ upholds a lower deformation in the MRZ than in the well-developed Okavango Graben. Several authors detected current displacements (Pastier et al., 2017; Wedmore et al., 2021) and neotectonic activity in the Okavango Graben, sometimes younger than 6 ka (Mokatse et al., 2022). This dynamics in the Okavango Graben contrasts with the very low deformation in the MRZ at least during the Holocene, but potentially for a longer time (this study). The magnitudes and distribution of earthquakes also supports a higher tectonic activity in the Okavango Graben than in the MRZ (Figure 13). Indeed, most of the seismicity in the Makgadikgadi Basin is located in its southern part and cannot be correlated to the faults of the MRZ. Most events have a magnitude <4 and cluster around mining areas, whereas the 2017 Mw 6.5 earthquake, located more than 100 km further south, is correlated to the reactivation of NW-SE Neoproterozoic faults related to the Zoetfontain Faults System (Kolawole et al., 2017; Mulabisana et al., 2021; Paulssen et al., 2022).

Most of the EARS active deformation is focused in the Okavango Graben and the Mid-Zambezi Rift (Dumisani, 2001), while the MRZ is poorly active, despite its structural continuity with the Mid-Zambezi Rift (Figure 13). We propose that the present-day deformation is transferred north of the MRZ from the Mid-Zambezi Rift to the Okavango Graben, forming a relay pattern between these two active grabens, bypassing the MRZ. The spatial layout of the Okavango Graben and the Mid-Zambezi Rift, which are parallel with a NE-SW lateral offset of their axes, is consistent with a relay configuration of the two grabens. Moreover, the E-W to NE-SW lineaments described in the remote sensing analysis join these two active rift structures where the density of the earthquakes decreases in the Mid-Zambezi Rift; while it increases in the Okavango Graben, south of the Mababe Depression (Figure 13). Hence, the orientation and the location of these lineaments suggest a transfer zone connecting the Okavango Graben and the Mid-Zambezi Rift. As mentioned before, this hypothesis has to be

confirmed based on field observations for the origin of the ENE-WSW to E-W lineaments, as they could also be related to Karoo or Proterozoic basement structures.

5.4. Dynamics of the Rift at Its Southwestern Terminus

The general WNW-ESE to NW-SE extension direction deduced from the fault analysis of the MRZ is consistent with data in other segments all along the Southwestern Branch of the EARS (e.g., Daly et al., 2020). In particular, all other grabens of the MOZB (the Okavango Graben and the Eiseb Graben), as well as the closest rift segments to the north (The Mid-Zambezi Rift, the Machili Graben and the Kafue Graben) also show significant active normal faults with similar NNE-SSW to NE-SW strikes.

However, several other data point that the current dynamics of the Southwestern Branch opening in the MOZB is more complex than a simple extensional model perpendicular to the orientation of the main normal faults. Indeed, geodetic data indicate that the Okavango Graben currently shows a dextral strike-slip displacement along a NE-SW direction (Pastier et al., 2017). At a larger scale, geodetic data reveal a complex displacement combining both a clockwise rotation and an E-W motion of the San plate relative to the Nubian plate (Malservisi et al., 2013; Wedmore et al., 2021). Both geodetic studies imply an extension direction oblique to the main NNE-SSW to NE-SW trending directions of normal faults in the MOZB. Kinabo et al. (2008) also suspected strike-slip displacements in the Okavango Graben based on fault pattern and offset of dykes imaged by aeromagnetic data. In contrast, the main NNE-SSW faults of the MRZ show only normal-dip displacements. However, unlike the Okavango Graben, faults of the MRZ are poorly active and thus not representative of the current dynamics of the EARS opening in the MOZB. Instead they could correspond to previous stages of the EARS opening with a mainly ESE-WNW to NE-SW extension direction, whereas current deformation accommodates displacements oblique to the main fault-strike. Another explanation could be strain partitioning in the system, where most of the strike-slip deformation would be accommodated at the western margin of the system (e.g., Gumare Fault system) whereas its eastern part only shows extensional deformation. Both hypothesis are compatible with our observations and more data would be needed to determine if one prevails.

5.5. Propagation of the Southwestern Branch of the Rift: A "Zip-Opening" Model

Daly et al. (2020) proposed that the Southwestern Branch of the EARS is propagating from northeast to southwest, forming an evolving plate boundary between the San and Nubian plates. They highlighted that the ages of fault initiation in the different rift segments decrease from Pliocene ages in the northeastern ones to Mid-Late Pleistocene ages in the southwestern ones (McCarthy, 2013; Moore et al., 2012; Wanke, 2005), showing a progressive opening of the rift from northeast to southwest. The lack of faults related to the EARS southwest of the Eiseb Graben also supports this hypothesis. Potential relationships between the EARS and the Walvis Ridge or with NNW trending faults in the Namibian Highlands were also proposed (Daly et al., 2020). Both hypotheses would imply a strong shift in the direction of the San-Nubian boundary that would take a WNW direction to reach the Walvis Ridge or a NNW direction to reach the faults in Namibia, almost perpendicular to the SW trend of the Southern Branch of the EARS. In both cases, there is a deformation gap (>300 km) between the Eiseb Graben and these structures, contrasting with the relative continuity of the Southwestern Branch from the Luangwa Rift to the Eiseb Graben (Figure 1a). This southwestward decrease in the opening of the Southwestern Branch of the rift implies that the northern region of the San plate moves away from the Nubian plate faster than its southern part, which is consistent with a clockwise rotation of San plate relative to the Nubian plate (Wedmore et al., 2021) (Figure 14a).

Based on the above arguments, we propose a "zip-opening" model for the EARS propagation at its southwestern terminus, that integrates the distribution of the deformation in the MOZB (Figure 14b). Rifting propagates from northeast to southwest, driven by the relative motion of San plate compared to the Nubian plate, combining a clockwise rotation and a southward drift. The clockwise rotation induces a main NW-SE extension and a NE-SW directed opening all along the southwestern rift, forming a succession of grabens parallel to each other. As the propagation evolves, the deformation localizes preferentially in some segments (e.g., the Okavango Graben and the Mid-Zambezi Rift) and decreases in others (e.g., the Makgadikgadi Basin). This results in the development of tectonic transfer zones between the active segments which accommodate these variations in the deformation. The drift of the San plate toward the south is accommodated along the Damara Belt boundary at the northwestern margin of the system by dextral strike-slip movements as shown by GNSS data (Figure 14a).

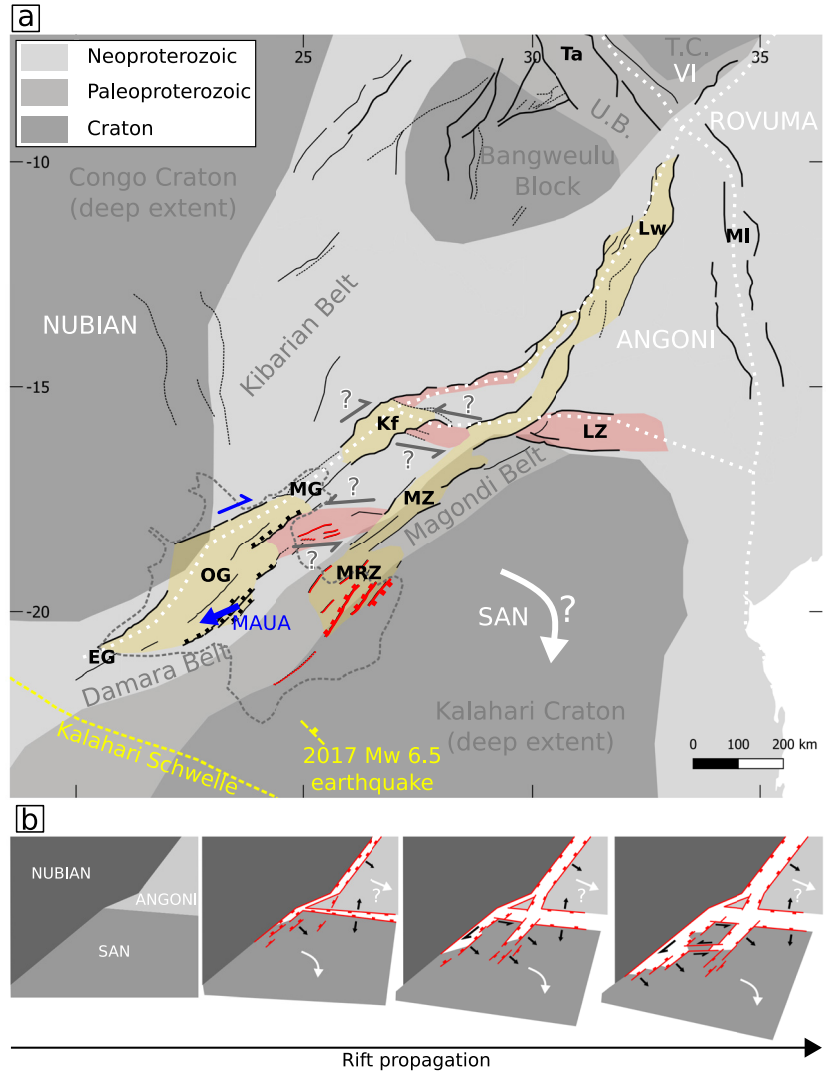

Figure 14. Kinematic model of the Southwestern Branch of the EARS. (a) Structural scheme of the Southwestern Branch of the EARS. The Precambrian basement map is modified from Gubanov and Mooney (2009) and Pastier et al. (2017) with block names given in gray—T.C., Tanzanian Craton; U.B., Ubendian Belt. Black annotations correspond to rift segments given in Figure 1. Light yellow areas correspond to NNE-SSW to NE-SW segments of the rift. Light red areas correspond to ENE-WSW to E-W segment of the rift. Black abbreviations correspond to rift segments: EG, Eiseb Graben; Kf, Kafue Graben; Lw, Luangwa Rift; LZ, Low-Zambezi Rift; MG, Machili Graben; Ml, Malawi Rift; MZ, Mid-Zambezi Rift; MRZ, Makgadikgadi Rift Zone; OG, Okavango Graben; Ta, Tanganyika Rift. Red faults correspond to this study. Black faults are compiled and modified from Chorowicz (2005) and Daly et al. (2020). Blue arrows are from Pastier et al. (2017) where MAUA arrow corresponds to Maun GPS station's average horizontal movement direction compared to Mongo and Rundu GPS stations (located on the Nubian plate). Gray arrows with question marks correspond to assumed fault kinematics from the model. The yellow dashed normal fault symbol is inferred from the 2017 Moiyabana M_w 6.5 earthquake by Mulabisana et al. (2021). The yellow dashed line corresponds to the ridge of the Kalahari Schwelle. Dashed white lines correspond to plate boundaries from Daly et al. (2020) with plate names given in white—VI, Victoria plate. The white arrow corresponds to San plate's movement relative to Nubian plate discussed in the text. Dotted gray contour delineates the MOZB. Question marks point hypothetic kinematics discussed in the text. (b) Schematic "zip-opening" model of the Southwestern Branch of the EARS. Faults are in red. White arrows correspond to plate movements where Nubian plate is considered stable. Black arrows indicate local kinematics assumed in the model.

An in-relay configuration of some rift segments linked by tectonic ENE-WSW to E-W transfer zones (between the Mid-Zambezi Rift and the Okavango Graben in this study) is consistent with a transtensional component predicted by the proposed model. Further investigations of the E-W to NE-SW lineaments joining the Okavango Graben and the Mid-Zambezi Rift and/or more geodetic data in and around the MOZB are thus necessary to

confirm the model. The WNW-ESE direction of the northern margin of the Kafue Graben could also be consistent with such a transfer zone between the Kafue Graben and the northern part of the Mid-Zambezi Rift (Figure 14a). Daly et al. (2020) recognized WNW transfer faults on the eastern margin of the Kafue Graben and suspected left-lateral oblique component on the E-W faults of the Kafue Graben, in agreement with this hypothesis.

Northeast of the Mid-Zambezi Rift, the E-W oriented Mesozoic Lower-Zambezi Rift (e.g., Oesterlen & Blenkinsop, 1994; Orpen et al., 1989), is considered as part of the boundary between the San and the Angoni plates (Daly et al., 2020) (Figure 14a). This boundary is poorly defined (Wedmore et al., 2021; Williams et al., 2021) and no current data exists about its present-day tectonic activity. Further investigation would be interesting as N-S extension at the northern margin of the San plate could fit with a southward directed rotational component of the San plate motion.

A propagating boundary between the San and Nubian plates, as proposed in the zip-opening model, raises the question of the accommodation of the San plate motion toward the south-southwest in the absence of a clear tectonic boundary. An alternative to it could be far field intraplate deformation south of the MOZB. The Mw 6.5 earthquake that occurred south of the Makgadikgadi Basin in 2017 (Figure 14a) supports the idea of intraplate deformation in this area (Kolawole et al., 2017; Mulabisana et al., 2021). The region south of the MOZB is also characterized by an axis of high elevations. In particular, the Kalahari Schwelle (Figure 14a) forms a WNW-ESE oriented topographic ridge more than 200 km wide and 400 km long south of the Makgadikgadi Basin, perpendicular with both EARS and basement structural directions. A late Paleogene flexure has been proposed for a related morphological axis of high elevations (Moore, 1999; Moore et al., 2009). However, the timing and the driver of the uplift of the Kalahari Schwelle itself remain poorly constrained. Both its localization and orientation would be consistent with an intraplate flexural uplift accommodating a clockwise rotation of the San plate.

6. Conclusion

The present morpho-structural study, conducted through remote sensing data analysis and field mapping, brings new constraints on the tectonic pattern at the southwestern terminus of the EARS. Due to the smooth topography and the almost-ubiquitous recent sediment cover, we analyzed the geomorphic features in the Makgadikgadi Basin. This analysis allowed us to define surface markers of fault kinematics and estimate the relative chronology of the rift deformation. Therefore, we demonstrate that the NNE-SSW faults of the MRZ are normal-dip, indicating that they formed under a roughly NW-SE to WNW-ESE directed extension regime. On the other hand, shorelines of Paleolake Makgadikgadi are not deformed by recent faulting. The integration of absolute ages from the literature to the established relative chronology shows that the MRZ had low to absent tectonic activity at least since early Holocene, which contrasts with the current activity of the adjacent Okavango Graben and Mid-Zambezi Rift. The spatial layout of rift segments, the earthquake distribution and the mapped lineaments and structural features suggest that the Okavango Graben and the Mid-Zambezi Rift are two in-relay segments of the EARS, which could explain the present-day low deformation in the MRZ. From our results and by integrating previous works, we propose a "zip-opening" model of the southwestern opening of the EARS, integrating the lack of deformation at the southwest of the Okavango and Eiseb grabens. This model describes an ongoing process of plate boundary propagation combining strike-slip and extension motions driven by the relative motion of the San plate compared to the Nubian plate.

Data Availability Statement

The GNSS data used for topographic profiles in the study are available at "GNSS data from fieldwork in northern Botswana (2021 and 2022 missions)" OSF repository via https://doi.org/10.17605/OSF.IO/43M8Z with CC-By Attribution 4.0 International license (Gaudaré et al., 2023). The Copernicus GLO-90 and GLO-30 data sets were used for topographic maps and topographic profiles, accessible at https://doi.org/10.5270/ESA-c5d3d65 (ESA, 2019). The Shuttle Radar Topography Mission (SRTM) 1 Arc-Second Global data set, accessible at https://doi.org/10.5066/F7PR7TFT was used for comparison with the Copernicus data sets (USGS EROS, 2018). International Seismological Centre on-line bulletin data set, accessible at https://doi.org/10.31905/D808B830, was used to display earthquakes (International Seismological Centre, 2022). Mapping, profiles plotting and data analysis were performed using the software QGIS version 3.16.16 (QGIS.org, 2022) and using the following python libraries: Geopandas version 0.10.2 (Jordahl et al., 2021), Matplotlib version 3.5.1 (Caswell et al., 2021; Hunter, 2007), Numpy version 1.21.5 (Harris et al., 2020) and Rasterio version 1.2.10 (Rasterio, 2022).

Acknowledgments
This work was granted by the CNRS (INSU-TELLUS program) and the University of Rennes, in the framework of the CNRS—GDR Rift. The fieldwork was conducted under the research permit ENT8/36/4L(83) kindly provided by the Ministry of Environment, Natural Resources Conservation and Tourism of Botswana. We thank the staff of the Okavango Research Institute as well as S. Corgne, D. Bavay and V. Mayombo for their great help with the fieldwork.

References

Baillieul, T. A. (1979). Makgadikgadi pans complex of central Botswana. *GSA Bulletin*, *90*(2_Part_II), 289–312. https://doi.org/10.1130/GSAB-P2-90-289

Begg, G. C., Griffin, W. L., Natapov, L. M., O'Reilly, S. Y., Grand, S. P., O'Neill, C. J., et al. (2009). The lithospheric architecture of Africa; seismic tomography, mantle petrology, and tectonic evolution. *Geosphere*, *5*(1), 23–50. https://doi.org/10.1130/GES00179.1

Bufford, K. M., Atekwana, E. A., Abdelsalam, M. G., Shemang, E., Atekwana, E. A., Mickus, K., et al. (2012). Geometry and faults tectonic activity of the Okavango Rift Zone, Botswana: Evidence from magnetotelluric and electrical resistivity tomography imaging. *Journal of African Earth Sciences*, *65*, 61–71. https://doi.org/10.1016/j.jafrearsci.2012.01.004

Burrough, S. L., Thomas, D. S. G., Allin, J. R., Coulson, S. D., Mothulatshipi, S. M., Nash, D. J., & Staurset, S. (2022). Lessons from a lakebed: Unpicking hydrological change and early human landscape use in the Makgadikgadi basin, Botswana. *Quaternary Science Reviews*, *291*, 107662. https://doi.org/10.1016/j.quascirev.2022.107662

Burrough, S. L., Thomas, D. S. G., & Bailey, R. M. (2009). Mega-Lake in the Kalahari: A Late Pleistocene record of the Palaeolake Makgadikgadi system. *Quaternary Science Reviews*, *28*(15), 1392–1411. https://doi.org/10.1016/j.quascirev.2009.02.007

Castaing, C. (1991). Post-Pan-African tectonic evolution of South Malawi in relation to the Karroo and recent East African rift systems. *Tectonophysics*, *191*(1–2), 55–73. https://doi.org/10.1016/0040-1951(91)90232-h

Caswell, T. A., Droettboom, M., Lee, A., Sales de Andrade, E., Hoffmann, T., Hunter, J., et al. (2021). matplotlib/matplotlib: REL: V3.5.1 [Software]. Zenodo. https://doi.org/10.5281/zenodo.5773480

Chorowicz, J. (2005). The East African rift system. *Journal of African Earth Sciences*, *43*(1–3), 379–410. https://doi.org/10.1016/j.jafrearsci.2005.07.019

Cooke, H. J. (1979). The origin of the Makgadikgadi Pans. *Botswana Notes and Records*, *11*, 37–42.

Cooke, H. J. (1980). Landform evolution in the context of climatic change and neo-tectonism in the Middle Kalahari of north-central Botswana. *Transactions of the Institute of British Geographers*, *5*(1), 80–99. https://doi.org/10.2307/622100

Cooke, H. J., & Verstappen, H. T. (1984). The landforms of the western Makgadikgadi basin in northern Botswana, with a consideration of the chronology of the evolution of Lake Palaeo-Makgadikgadi. *Zeitschrift für Geomorphologie*, *28*(1), 1–19. https://doi.org/10.1127/zfg/28/1984/1

Daly, M. C., Chorowicz, J., & Fairhead, J. D. (1989). Rift basin evolution in Africa: The influence of reactivated steep basement shear zones. *Geological Society, London, Special Publications*, *44*(1), 309–334. https://doi.org/10.1144/GSL.SP.1989.044.01.17

Daly, M. C., Green, P., Watts, A. B., Davies, O., Chibesakunda, F., & Walker, R. (2020). Tectonics and landscape of the Central African Plateau and their implications for a propagating Southwestern Rift in Africa. *Geochemistry, Geophysics, Geosystems*, *21*(6), e2019GC008746. https://doi.org/10.1029/2019GC008746

Dauteuil, O. (1995). Fault pattern from Seabeam processing: The Western part of the Blanco fracture Zone (NE Pacific). *Marine Geophysical Researches*, *17*(1), 17–35. https://doi.org/10.1007/BF01268049

Dauteuil, O., Picart, C., Guillocheau, F., Pickford, M., & Senut, B. (2018). Cenozoic deformation and geomorphic evolution of the Sperrgebiet area (Southern Namibia). *Communications of the Geological Survey of Namibia*, *18*, 1–18.

Dumisani, J. H. (2001). Seismotectonics of Zimbabwe. *African Journal of Science and Technology*, *1*(4), 22–28. https://doi.org/10.4314/ajst.v1i4.44622

Du Toit, A. L. (1927). The Kalahari and some of its problems. *South African Journal of Science*, *24*, 88–101.

Eckardt, F. D., Bryant, R. G., McCulloch, G., Spiro, B., & Wood, W. W. (2008). The hydrochemistry of a semi-arid pan basin case study: Sua Pan, Makgadikgadi, Botswana. *Applied Geochemistry*, *23*(6), 1563–1580. https://doi.org/10.1016/j.apgeochem.2007.12.033

Eckardt, F. D., Cotterill, F. P. D., Flügel, T. J., Kahle, B., McFarlane, M., & Rowe, C. (2016). Mapping the surface geomorphology of the Makgadikgadi Rift Zone (MRZ). *Quaternary International*, *404*, 115–120. https://doi.org/10.1016/j.quaint.2015.09.002

ESA. (2019). Copernicus DEM - Global and European Digital Elevation Model (COP-DEM) [Dataset]. European Spatial Agency (ESA). https://doi.org/10.5270/ESA-c5d3d65

Fahrland, E., Jacob, P., Schrader, H., & Kahabka, H. (2020). Copernicus DEM - handbook document. Retrieved from https://spacedata.copernicus.eu/documents/20126/0/GEO1988-CopernicusDEM-SPE-002_ProductHandbook_I1.00.pdf

Fairhead, J. D., & Stuart, G. W. (1982). The seismicity of the East African rift system and comparison with other continental rifts. In *Continental and Oceanic Rifts* (pp. 41–61). American Geophysical Union (AGU). https://doi.org/10.1029/GD008p0041

Franchi, F., Cavalazzi, B., Evans, M., Filippidou, S., Mackay, R., Malaspina, P., et al. (2022). Late Pleistocene–Holocene palaeoenvironmental evolution of the Makgadikgadi Basin, Central Kalahari, Botswana: New evidence from shallow sediments and ostracod fauna. *Frontiers in Ecology and Evolution*, *10*, 818417. https://doi.org/10.3389/fevo.2022.818417

Franchi, F., Kelepile, T., Di Capua, A., De Wit, M. C. J., Kemiso, O., Lasarwe, R., & Catuneanu, O. (2021). Lithostratigraphy, sedimentary petrography and geochemistry of the upper Karoo Supergroup in the central Kalahari Karoo sub-basin, Botswana. *Journal of African Earth Sciences*, *173*, 104025. https://doi.org/10.1016/j.jafrearsci.2020.104025

Franchi, F., MacKay, R., Selepeng, A. T., & Barbieri, R. (2020). Layered mound, inverted channels and polygonal fractures from the Makgadikgadi pan (Botswana): Possible analogues for Martian aqueous morphologies. *Planetary and Space Science*, *192*, 105048. https://doi.org/10.1016/j.pss.2020.105048

Garzanti, E., Pastore, G., Stone, A., Vainer, S., Vermeesch, P., & Resentini, A. (2022). Provenance of Kalahari Sand: Paleoweathering and recycling in a linked fluvial-aeolian system. *Earth-Science Reviews*, *224*, 103867. https://doi.org/10.1016/j.earscirev.2021.103867

Gaudaré, L., Dauteuil, O., & Jolivet, M. (2023). GNSS data from fieldwork in northern Botswana (2021 and 2022 missions) [Dataset]. OSF. https://doi.org/10.17605/OSF.IO/43M8Z

Grey, D. R. C., & Cooke, H. J. (1977). Some problems in the quaternary evolution of the landforms of northern Botswana. *Catena*, *4*(1), 123–133. https://doi.org/10.1016/0341-8162(77)90014-5

Grove, A. T. (1969). Landforms and climatic change in the Kalahari and Ngamiland. *The Geographical Journal*, *135*(2), 191. https://doi.org/10.2307/1796824

Gubanov, A. P., & Mooney, W. D. (2009). New global geological maps of crustal basement age. In *American Geophysical Union, Fall Meeting 2009*. Retrieved from https://ui.adsabs.harvard.edu/abs/2009AGUFM.T53B1583G

Guillocheau, F., Simon, B., Baby, G., Bessin, P., Robin, C., & Dauteuil, O. (2018). Planation surfaces as a record of mantle dynamics: The case example of Africa. *Gondwana Research*, *53*, 82–98. https://doi.org/10.1016/j.gr.2017.05.015

Gumbricht, T., McCarthy, T. S., & Merry, C. L. (2001). The topography of the Okavango Delta, Botswana, and its tectonic and sedimentological implications. *South African Journal of Geology*, *104*(3), 243–264. https://doi.org/10.2113/1040243

Haddon, I. G. (2005). The Sub-Kalahari geology and tectonic evolution of the Kalahari basin, Southern Africa [Thesis]. Retrieved from http://wiredspace.wits.ac.za/handle/10539/193

Haddon, I. G., & McCarthy, T. S. (2005). The Mesozoic-Cenozoic interior sag basins of Central Africa: The Late Cretaceous-Cenozoic Kalahari and Okavango basins. *Journal of African Earth Sciences*, *43*(1–3), 316–333. https://doi.org/10.1016/j.jafrearsci.2005.07.008

Harris, C. R., Millman, K. J., Van der Walt, S. J., Gommers, R., Virtanen, P., Cournapeau, D., et al. (2020). Array programming with NumPy. *Nature*, *585*(7825), 357–362. https://doi.org/10.1038/s41586-020-2649-2

Hasterok, D., Halpin, J. A., Collins, A. S., Hand, M., Kreemer, C., Gard, M. G., & Glorie, S. (2022). New maps of global geological provinces and tectonic plates. *Earth-Science Reviews*, *231*, 104069. https://doi.org/10.1016/j.earscirev.2022.104069

Hlatywayo, J. D. (1995). Fault-plane solutions of the Deka Fault zone and mid-Zambezi Valley. *Geophysical Journal International*, *120*(3), 567–576. https://doi.org/10.1111/j.1365-246X.1995.tb01839.x

Hollands, C. B., Nanson, G. C., Jones, B. G., Bristow, C. S., Price, D. M., & Pietsch, T. J. (2006). Aeolian–fluvial interaction: Evidence for Late Quaternary channel change and wind-rift linear dune formation in the northwestern Simpson Desert, Australia. *Quaternary Science Reviews*, *25*(1), 142–162. https://doi.org/10.1016/j.quascirev.2005.02.007

Hunter, J. D. (2007). Matplotlib: A 2D graphics environment. *Computing in Science & Engineering*, *9*(3), 90–95. https://doi.org/10.1109/MCSE.2007.55

International Seismological Centre. (2022). On-line bulletin [Dataset]. International Seismological Centre (ICS). https://doi.org/10.31905/D808B830

Jolivet, M., Dauteuil, O., & Gaudaré, L. (2022). Blowing the rivers: Regional-scale control of the drainage network by wind in northern Kalahari (Africa). *Geomorphology*, *398*, 108039. https://doi.org/10.1016/j.geomorph.2021.108039

Jordahl, K., Van den Bossche, J., Fleischmann, M., McBride, J., Wasserman, J., Garcia Badaracco, A., et al. (2021). geopandas/geopandas: V0.10.2 [Software]. Zenodo. https://doi.org/10.5281/zenodo.5573592

Jourdan, F., Féraud, G., Bertrand, H., Kampunzu, A. B., Tshoso, G., Le Gall, B., et al. (2004). The Karoo triple junction questioned: Evidence from Jurassic and Proterozoic $^{40}Ar/^{39}Ar$ ages and geochemistry of the giant Okavango dyke swarm (Botswana). *Earth and Planetary Science Letters*, *222*(3–4), 989–1006. https://doi.org/10.1016/j.epsl.2004.03.017

Jourdan, F., Féraud, G., Bertrand, H., Kampunzu, A. B., Tsoho, G., Watkeys, M. K., & Le Gall, B. (2005). Karoo large igneous province: Brevity, origin, and relation to mass extinction questioned by new $^{40}Ar/^{39}Ar$ age data. *Geology*, *33*(9), 745–748. https://doi.org/10.1130/G21632.1

Jourdan, F., Féraud, G., Bertrand, H., Watkeys, M. K., Kampunzu, A. B., & Le Gall, B. (2006). Basement control on dyke distribution in Large Igneous Provinces: Case study of the Karoo triple junction. *Earth and Planetary Science Letters*, *241*(1–2), 307–322. https://doi.org/10.1016/j.epsl.2005.10.003

Key, R. M., & Ayres, N. (2000). The 1998 edition of the national geological map of Botswana. *Journal of African Earth Sciences*, *30*(3), 427–451. https://doi.org/10.1016/S0899-5362(00)00030-0

Khoza, T. D., Jones, A. G., Muller, M. R., Evans, R. L., Miensopust, M. P., & Webb, S. J. (2013). Lithospheric structure of an Archean craton and adjacent mobile belt revealed from 2-D and 3-D inversion of magnetotelluric data: Example from southern Congo craton in northern Namibia. *Journal of Geophysical Research: Solid Earth*, *118*(8), 4378–4397. https://doi.org/10.1002/jgrb.50258

Kinabo, B. D., Atekwana, E. A., Hogan, J. P., Modisi, M. P., Wheaton, D. D., & Kampunzu, A. B. (2007). Early structural development of the Okavango rift zone, NW Botswana. *Journal of African Earth Sciences*, *48*(2–3), 125–136. https://doi.org/10.1016/j.jafrearsci.2007.02.005

Kinabo, B. D., Hogan, J. P., Atekwana, E. A., Abdelsalam, M. G., & Modisi, M. P. (2008). Fault growth and propagation during incipient continental rifting: Insights from a combined aeromagnetic and Shuttle Radar Topography Mission digital elevation model investigation of the Okavango Rift Zone, northwest Botswana. *Tectonics*, *27*(3), TC3013. https://doi.org/10.1029/2007TC002154

Kleusberg, A. (1986). Kinematic relative positioning using GPS code and carrier beat phase observations. *Marine Geodesy*, *10*(3–4), 257–274. https://doi.org/10.1080/01490418609388025

Kolawole, F., Atekwana, E. A., Malloy, S., Stamps, D. S., Grandin, R., Abdelsalam, M. G., et al. (2017). Aeromagnetic, gravity, and Differential Interferometric Synthetic Aperture Radar analyses reveal the causative fault of the 3 April 2017 Mw 6.5 Moiyabana, Botswana, earthquake. *Geophysical Research Letters*, *44*(17), 8837–8846. https://doi.org/10.1002/2017GL074620

Lancaster, I. N. (1978). The pans of the southern Kalahari, Botswana. *The Geographical Journal*, *144*(1), 81–98. https://doi.org/10.2307/634651

Lancaster, I. N. (1982). Linear dunes. *Progress in Physical Geography: Earth and Environment*, *6*(4), 475–504. https://doi.org/10.1177/030913338200600401

Lawson, M. P., & Thomas, D. S. G. (2002). Late Quaternary lunette dune sedimentation in the southwestern Kalahari Desert, South Africa: Luminescence based chronologies of aeolian activity. *Quaternary Science Reviews*, *21*(7), 825–836. https://doi.org/10.1016/S0277-3791(01)00131-7

Le Gall, B., Tshoso, G., Dyment, J., Basira Kampunzu, A., Jourdan, F., Féraud, G., et al. (2005). The Okavango giant mafic dyke swarm (NE Botswana): Its structural significance within the Karoo Large Igneous Province. *Journal of Structural Geology*, *27*(12), 2234–2255. https://doi.org/10.1016/j.jsg.2005.07.004

Le Gall, B., Tsoho, G., Jourdan, F., Féraud, G., Bertrand, H., Tiercelin, J. J., et al. (2002). $^{40}Ar/^{39}Ar$ geochronology and structural data from the giant Okavango and related mafic dyke swarms, Karoo igneous province, northern Botswana. *Earth and Planetary Science Letters*, *202*, 596–606.

Livingstone, I. (1988). New models for the formation of linear sand dunes. *Geography*, *73*(2), 105–115.

Macgregor, D. (2015). History of the development of the East African Rift System: A series of interpreted maps through time. *Journal of African Earth Sciences*, *101*, 232–252. https://doi.org/10.1016/j.jafrearsci.2014.09.016

Malservisi, R., Hugentobler, U., Wonnacott, R., & Hackl, M. (2013). How rigid is a rigid plate? Geodetic constraint from the TrigNet CGPS network, South Africa. *Geophysical Journal International*, *192*(3), 918–928. https://doi.org/10.1093/gji/ggs081

Martin, A. K. (2023). Opposite microplate rotations on the East African Rift: Similarity to double saloon door tectonics. *Journal of African Earth Sciences*, *198*, 104803. https://doi.org/10.1016/j.jafrearsci.2022.104803

McCarthy, T. S. (2013). The Okvango Delta and its place in the geomorphological evolution of Southern Africa. *South African Journal of Geology*, *116*(1), 1–54. https://doi.org/10.2113/gssajg.116.1.1

McCarthy, T. S., Green, R. W., & Franey, N. J. (1993). The influence of neo-tectonics on water dispersal in the northeastern regions of the Okavango swamps, Botswana. *Journal of African Earth Sciences*, *17*(1), 23–32. https://doi.org/10.1016/0899-5362(93)90019-M

McFarlane, M. J., & Eckardt, F. D. (2007). Palaeodune morphology associated with the Gumare fault of the Okavango graben in the Botswana/Namibia borderland: A new model of tectonic influence. *South African Journal of Geology*, *110*(4), 535–542. https://doi.org/10.2113/gssajg.110.4.535

McFarlane, M. J., & Eckardt, F. D. (2008). Lake deception: A new Makgadikgadi palaeolake. *Botswana Notes and Records*, *38*(1), 195–201. https://doi.org/10.10520/AJA052550590_217

McFarlane, M. J., Eckardt, F. D., Ringrose, S., Coetzee, S. H., & Kuhn, J. R. (2005). Degradation of linear dunes in Northwest Ngamiland, Botswana and the implications for luminescence dating of periods of aridity. *Quaternary International*, *135*(1), 83–90. https://doi.org/10.1016/j.quaint.2004.10.025

Miensopust, M. P., Jones, A. G., Muller, M. R., Garcia, X., & Evans, R. L. (2011). Lithospheric structures and Precambrian terrane boundaries in northeastern Botswana revealed through magnetotelluric profiling as part of the Southern African Magnetotelluric Experiment. *Journal of Geophysical Research*, *116*(B2), B02401. https://doi.org/10.1029/2010JB007740

Miller, R. M., Pickford, M., & Senut, B. (2010). The geology, palaeontology and evolution of the Etosha Pan, Namibia: Implications for terminal Kalahari deposition. *South African Journal of Geology*, *113*(3), 307–334. https://doi.org/10.2113/gssajg.113.3.307

Modisi, M. P. (2000). Fault system of the southeastern boundary of the Okavango Rift, Botswana. *Journal of African Earth Sciences*, *30*(3), 569–578. https://doi.org/10.1016/S0899-5362(00)00039-7

Mokatse, T., Vainer, S., Irving, J., Schmidt, C., Kgosidintsi, B., Shemang, E., & Verrecchia, E. P. (2022). Geometry of sedimentary deposits and evolution of the landforms in the Chobe Enclave, Northern Botswana. *Geomorphology*, *415*, 108406. https://doi.org/10.1016/j.geomorph.2022.108406

Moore, A., Blenkinsop, T., & Cotterill, F. (2009). Southern African topography and erosion history: Plumes or plate tectonics? *Terra Nova*, *21*(4), 310–315. https://doi.org/10.1111/j.1365-3121.2009.00887.x

Moore, A. E. (1999). A reappraisal of epeirogenic flexure axes in Southern Africa. *South African Journal of Geology*, *102*(4), 363–376.

Moore, A. E. (2013). Anatomy of a distal kimberlite indicator mineral (KIM) anomaly in the Central Kalahari, Botswana. *South African Journal of Geology*, *116*(1), 67–78. https://doi.org/10.2113/gssajg.116.1.67

Moore, A. E., Cotterill, F. P. D., & Eckardt, F. D. (2012). The evolution and ages of Makgadikgadi palaeo-lakes: Consilient evidence from Kalahari drainage evolution south-central Africa. *South African Journal of Geology*, *115*(3), 385–413. https://doi.org/10.2113/gssajg.115.3.385

Moore, A. E., & Larkin, P. A. (2001). Drainage evolution in south-central Africa since the breakup of Gondwana. *South African Journal of Geology*, *104*(1), 47–68. https://doi.org/10.2113/104.1.47

Morley, C. K. (2010). Stress re-orientation along zones of weak fabrics in rifts: An explanation for pure extension in 'oblique' rift segments? *Earth and Planetary Science Letters*, *297*(3), 667–673. https://doi.org/10.1016/j.epsl.2010.07.022

Mulabisana, T., Meghraoui, M., Midzi, V., Saleh, M., Ntibinyane, O., Kwadiba, T., et al. (2021). Seismotectonic analysis of the 2017 Moiyabana earthquake (MW 6.5; Botswana), insights from field investigations, aftershock and InSAR studies. *Journal of African Earth Sciences*, *182*, 104297. https://doi.org/10.1016/j.jafrearsci.2021.104297

Muller, M. R., Jones, A. G., Evans, R. L., Grütter, H. S., Hatton, C., Garcia, X., et al. (2009). Lithospheric structure, evolution and diamond prospectivity of the Rehoboth Terrane and western Kaapvaal Craton, southern Africa: Constraints from broadband magnetotellurics. *Lithos*, *112*, 93–105. https://doi.org/10.1016/j.lithos.2009.06.023

Nthaba, B., Simon, R. E., & Ogubazghi, G. M. (2018). Seismicity study of Botswana from 1966 to 2012. *International Journal of Geosciences*, *9*(12), 707–718. https://doi.org/10.4236/ijg.2018.912043

Nyblade, A. A., & Robinson, S. W. (1994). The African Superswell. *Geophysical Research Letters*, *21*(9), 765–768. https://doi.org/10.1029/94GL00631

Oesterlen, P. M., & Blenkinsop, T. G. (1994). Extension directions and strain near the failed triple junction of the Zambezi and Luangwa Rift zones, southern Africa. *Journal of African Earth Sciences*, *18*(2), 175–180. https://doi.org/10.1016/0899-5362(94)90029-9

O'Leary, D. W., Friedman, J. D., & Pohn, H. A. (1976). Lineament, linear, lineation: Some proposed new standards for old terms. *GSA Bulletin*, *87*(10), 1463–1469. https://doi.org/10.1130/0016-7606(1976)87<1463:LLLSPN>2.0.CO;2

Orpen, J. L., Swain, C. J., Nugent, C., & Zhou, P. P. (1989). Wrench-fault and half-graben tectonics in the development of the Palaeozoic Zambezi Karoo Basins in Zimbabwe—The "Lower Zambezi" and "Mid-Zambezi" basins respectively—And regional implications. *Journal of African Earth Sciences*, *8*(2), 215–229. https://doi.org/10.1016/S0899-5362(89)80026-0

Otvos, E. G. (2000). Beach ridges—Definitions and significance. *Geomorphology*, *32*(1), 83–108. https://doi.org/10.1016/S0169-555X(99)00075-6

Pastier, A. M., Dauteuil, O., Murray-Hudson, M., Moreau, F., Walpersdorf, A., & Makati, K. (2017). Is the Okavango Delta the terminus of the East African Rift System? Towards a new geodynamic model: Geodetic study and geophysical review. *Tectonophysics*, *712–713*, 469–481. https://doi.org/10.1016/j.tecto.2017.05.035

Paulssen, H., Micallef, T., Bouwman, D. R., Ruigrok, E., Herman, M. W., Fadel, I., et al. (2022). Rifting of the Kalahari Craton through Botswana? New seismic evidence. *Journal of Geophysical Research: Solid Earth*, *127*(4), e2021JB023524. https://doi.org/10.1029/2021JB023524

Podgorski, J. E., Green, A. G., Kgotlhang, L., Kinzelbach, W. K. H., Kalscheuer, T., Auken, E., & Ngwisanyi, T. (2013). Paleo-megalake and paleo-megafan in southern Africa. *Geology*, *41*(11), 1155–1158. https://doi.org/10.1130/G34735.1

QGIS.org. (2022). QGIS Geographic Information System (version 3.16.16) [Software]. QGIS Association. Retrieved from http://www.qgis.org

Rasterio. (2022). rasterio/rasterio (version 1.2.10) [Software]. GitHub. Retrieved from https://github.com/rasterio/rasterio

Reeves, C. V. (1972a). Earthquakes in Ngamiland. *Botswana Notes and Records*, *4*, 257–261.

Reeves, C. V. (1972b). Rifting in the Kalahari? *Nature*, *237*(5350), 95–96. https://doi.org/10.1038/237095a0

Riedel, F., Henderson, A. C. G., Heußner, K.-U., Kaufmann, G., Kossler, A., Leipe, C., et al. (2014). Dynamics of a Kalahari long-lived mega-lake system: Hydromorphological and limnological changes in the Makgadikgadi Basin (Botswana) during the terminal 50 ka. *Hydrobiologia*, *739*(1), 25–53. https://doi.org/10.1007/s10750-013-1647-x

Ringrose, S., Harris, C., Huntsman-Mapila, P., Vink, B. W., Diskins, S., Vanderpost, C., & Matheson, W. (2009). Origins of strandline duricrusts around the Makgadikgadi Pans (Botswana Kalahari) as deduced from their chemical and isotope composition. *Sedimentary Geology*, *219*(1), 262–279. https://doi.org/10.1016/j.sedgeo.2009.05.021

Ringrose, S., Huntsman-Mapila, P., Downey, W., Coetzee, S., Fey, M., Vanderpost, C., et al. (2008). Diagenesis in Okavango fan and adjacent dune deposits with implications for the record of palaeo-environmental change in Makgadikgadi–Okavango–Zambezi basin, northern Botswana. *Geomorphology*, *101*(4), 544–557. https://doi.org/10.1016/j.geomorph.2008.02.008

Ringrose, S., Huntsman-Mapila, P., Kampunzu, A. B., Downey, W., Coetzee, S., Vink, B., et al. (2005). Sedimentological and geochemical evidence for palaeo-environmental change in the Makgadikgadi subbasin, in relation to the MOZ rift depression, Botswana. *Palaeogeography, Palaeoclimatology, Palaeoecology*, *217*(3), 265–287. https://doi.org/10.1016/j.palaeo.2004.11.024

Saria, E., Calais, E., Stamps, D. S., Delvaux, D., & Hartnady, C. J. H. (2014). Present-day kinematics of the East African Rift. *Journal of Geophysical Research: Solid Earth*, *119*(4), 3584–3600. https://doi.org/10.1002/2013JB010901

Scheiber, T., Fredin, O., Viola, G., Jarna, A., Gasser, D., & Łapińska-Viola, R. (2015). Manual extraction of bedrock lineaments from high-resolution LiDAR data: Methodological bias and human perception. *GFF*, *137*(4), 362–372. https://doi.org/10.1080/11035897.2015.1085434

Schmidt, M., Fuchs, M., Henderson, A. C. G., Kossler, A., Leng, M. J., Mackay, A. W., et al. (2017). Paleolimnological features of a mega-lake phase in the Makgadikgadi Basin (Kalahari, Botswana) during Marine Isotope Stage 5 inferred from diatoms. *Journal of Paleolimnology*, *58*(3), 373–390. https://doi.org/10.1007/s10933-017-9984-9

Scholz, C. H., Koczynski, T. A., & Hutchin, D. G. (1976). Evidence of the incipient rifting in southern Africa. *Geophysical Journal of the Royal Astronomical Society*, *44*(1), 135–144. https://doi.org/10.1111/j.1365-246X.1976.tb00278.x

Schwarz, K. P., Cannon, M. E., & Wong, R. V. C. (1989). A comparison of GPS kinematics models for the determination of position and velocity along a trajectory. *Manuscripta Geodetica*, *14*, 345–353.
Shaw, P. A. (1988). After the flood: The fluvio-lacustrine landforms of Northern Botswana. *Earth-Science Reviews*, *25*(5), 449–456. https://doi.org/10.1016/0012-8252(88)90011-6
Shaw, P. A. (1997). Africa and Europe. In D. S. G. Thomas (Éd.), *Arid zone geomorphology: Process, form and change in drylands* (2nd ed., pp. 467–485). John Wiley & Sons Ltd.
Shaw, P. A., Thomas, D. S. G., & Nash, D. J. (1992). Late Quaternary fluvial activity in the dry valleys (mekgacha) of the Middle and Southern Kalahari, southern Africa. *Journal of Quaternary Science*, *7*(4), 273–281. https://doi.org/10.1002/jqs.3390070402
Simon, B. (2015). *Rift du Lac Albert, Ouganda, Rift Est Africain: Déformation, érosion, sédimentation et bilan de matière depuis 17 Ma* [PhD thesis]. Université Rennes 1. Retrieved from https://tel.archives-ouvertes.fr/tel-01923327
Singletary, S. J., Hanson, R. E., Martin, M. W., Crowley, J. L., Bowring, S. A., Key, R. M., et al. (2003). Geochronology of basement rocks in the Kalahari Desert, Botswana, and implications for regional Proterozoic tectonics. *Precambrian Research*, *121*(1–2), 47–71. https://doi.org/10.1016/S0301-9268(02)00201-2
Smith, M. J., & Clark, C. D. (2005). Methods for the visualization of digital elevation models for landform mapping. *Earth Surface Processes and Landforms*, *30*(7), 885–900. https://doi.org/10.1002/esp.1210
Stamps, D. S., Calais, E., Saria, E., Hartnady, C., Nocquet, J.-M., Ebinger, C. J., & Fernandes, R. M. (2008). A kinematic model for the East African Rift. *Geophysical Research Letters*, *35*(5), L05304. https://doi.org/10.1029/2007GL032781
Stamps, D. S., Kreemer, C., Fernandes, R., Rajaonarison, T. A., & Rambolamanana, G. (2021). Redefining East African Rift System kinematics. *Geology*, *49*(2), 150–155. https://doi.org/10.1130/G47985.1
Stokes, S., Haynes, G., Thomas, D. S. G., Horrocks, J. L., Higginson, M., & Malifa, M. (1998). Punctuated aridity in southern Africa during the last glacial cycle: The chronology of linear dune construction in the northeastern Kalahari. *Palaeogeography, Palaeoclimatology, Palaeoecology*, *137*(3), 305–322. https://doi.org/10.1016/S0031-0182(97)00106-5
Stokes, S., Thomas, D. S. G., & Shaw, P. A. (1997). New chronological evidence for the nature and timing of linear dune development in the southwest Kalahari Desert. *Geomorphology*, *20*(1), 81–93. https://doi.org/10.1016/S0169-555X(97)00006-8
Stone, A. (2021). Dryland dunes and other dryland environmental archives as proxies for Late Quaternary stratigraphy and environmental and climate change in southern Africa. *South African Journal of Geology*, *124*(4), 927–962. https://doi.org/10.25131/sajg.124.0055
Telfer, M. W., & Thomas, D. S. G. (2007). Late Quaternary linear dune accumulation and chronostratigraphy of the southwestern Kalahari: Implications for aeolian palaeoclimatic reconstructions and predictions of future dynamics. *Quaternary Science Reviews*, *26*(19), 2617–2630. https://doi.org/10.1016/j.quascirev.2007.07.006
Thomas, D. S. G. (1984). Ancient ergs of the former arid zones of Zimbabwe, Zambia and Angola. *Transactions of the Institute of British Geographers*, *9*(1), 75. https://doi.org/10.2307/621868
Thomas, D. S. G., & Burrough, S. L. (2016). Luminescence-based dune chronologies in southern Africa: Analysis and interpretation of dune database records across the subcontinent. *Quaternary International*, *410*, 30–45. https://doi.org/10.1016/j.quaint.2013.09.008
Thomas, D. S. G., & Shaw, P. A. (1991). *The Kalahari environment* (p. 284). Cambridge University Press.
Tsoar, H., Blumberg, D. G., & Stoler, Y. (2004). Elongation and migration of sand dunes. *Geomorphology*, *57*(3), 293–302. https://doi.org/10.1016/S0169-555X(03)00161-2
USGS EROS. (2018). Shuttle Radar Topography Mission 1 Arc-Second Global [Dataset]. United States Geological Survey (USGS) Earth Resources Observation and Science (EROS) Center. https://doi.org/10.5066/F7PR7TFT
Vail, J. R. (1968). The southern extension of the East African Rift System and related igneous activity. *Geologische Rundschau*, *57*(2), 601–614. https://doi.org/10.1007/BF01821264
Van Der Beek, P., Mbede, E., Andriessen, P., & Delvaux, D. (1998). Denudation history of the Malawi and Rukwa Rift flanks (East African Rift System) from apatite fission track thermochronology. *Journal of African Earth Sciences*, *26*(3), 363–385. https://doi.org/10.1016/S0899-5362(98)00021-9
Wanke, H. (2005). The Namibian Eiseb Graben as an extension of the East African Rift: Evidence from Landsat TM5 imagery. *South African Journal of Geology*, *108*(4), 541–546. https://doi.org/10.2113/108.4.541
Wedmore, L. N. J., Biggs, J., Floyd, M., Fagereng, Å., Mdala, H., Chindandali, P., et al. (2021). Geodetic constraints on cratonic microplates and broad strain during rifting of thick Southern African lithosphere. *Geophysical Research Letters*, *48*(17), e2021GL093785. https://doi.org/10.1029/2021GL093785
Wiles, J. W. (1971). *Rhodesia Geological 1:1000000* [Map] (6th ed.). Rhodesia Geological Survey.
Williams, J. N., Mdala, H., Fagereng, Å., Wedmore, L. N. J., Biggs, J., Dulanya, Z., et al. (2021). A systems-based approach to parameterise seismic hazard in regions with little historical or instrumental seismicity: Active fault and seismogenic source databases for southern Malawi. *Solid Earth*, *12*(1), 187–217. https://doi.org/10.5194/se-12-187-2021
Youssof, M., Thybo, H., Artemieva, I. M., & Levander, A. (2013). Moho depth and crustal composition in Southern Africa. *Tectonophysics*, *609*, 267–287. https://doi.org/10.1016/j.tecto.2013.09.001